



Optimized inhaled LNP formulation for enhanced treatment of idiopathic pulmonary fibrosis via mRNA-mediated antibody therapy

Received: 3 January 2024

Accepted: 24 July 2024

Published online: 10 August 2024

 Check for updates

Xin Bai^{1,2}, Qijing Chen^{1,2}, Fengqiao Li^{3,4}, Yilong Teng^{1,2}, Maoping Tang^{1,2}, Jia Huang^{1,2}, Xiaoyang Xu^{3,4}  & Xue-Qing Zhang^{1,2} 

Lipid nanoparticle-assisted mRNA inhalation therapy necessitates addressing challenges such as resistance to shear force damage, mucus penetration, cellular internalization, rapid lysosomal escape, and target protein expression. Here, we introduce the innovative “LOOP” platform with a four-step workflow to develop inhaled lipid nanoparticles specifically for pulmonary mRNA delivery. iLNP-HP08^{LOOP} featuring a high helper lipid ratio, acidic dialysis buffer, and excipient-assisted nebulization buffer, demonstrates exceptional stability and enhanced mRNA expression in the lungs. By incorporating mRNA encoding IL-11 single chain fragment variable (scFv), scFv@iLNP-HP08^{LOOP} effectively delivers and secretes IL-11 scFv to the lungs of male mice, significantly inhibiting fibrosis. This formulation surpasses both inhaled and intravenously injected IL-11 scFv in inhibiting fibroblast activation and extracellular matrix deposition. The HP08^{LOOP} system is also compatible with commercially available ALC0315 LNPs. Thus, the “LOOP” method presents a powerful platform for developing inhaled mRNA nanotherapeutics with potential for treating various respiratory diseases, including idiopathic pulmonary fibrosis.

Interstitial lung diseases (ILDs) encompass a range of disorders characterized by varying degrees of inflammation and scarring¹. One of the most common forms is idiopathic pulmonary fibrosis (IPF), a fibrotic-predominant ILD distinguished by extensive fibrotic lesions and a higher mortality rate than many cancers². Typically, IPF occurs when damaged epithelial cells repair abnormally, resulting in scar formation in the lungs' gas exchange region³. Numerous factors, such as viral infections, smoking, environmental exposure, gastroesophageal reflux, and aging, have been identified as potential triggers for epithelial cell injury^{4,5}. Currently, the only available treatments for IPF are

pirfenidone and nintedanib, which can slow disease progression but cannot reverse scarring. Multiple drugs, including PRM-151⁶, treprostinil (Tyvaso)⁷, and N-acetylcysteine⁸, are currently in clinical trials, offering hope for future treatment options.

mRNA-based protein replacement therapy holds immense promise, enabling the expression of any required protein or peptide^{9,10}, targeting “undruggable” targets, avoiding insertional mutagenesis, triggering long-term protein expression, creating therapeutic antibody cocktails, and accelerating development cycles^{11–14}. This offers significant hope for immunizing against various viruses and treating

¹Shanghai Frontiers Science Center of Drug Target Identification and Delivery, School of Pharmaceutical Sciences, Shanghai Jiao Tong University, Shanghai, China. ²National Key Laboratory of Innovative Immunotherapy, Shanghai Jiao Tong University, Shanghai, China. ³Department of Chemical and Materials Engineering, New Jersey Institute of Technology, Newark, NJ, USA. ⁴Department of Biomedical Engineering, New Jersey Institute of Technology, Newark, NJ, USA. ✉e-mail: xiaoyang.xu@njit.edu; xueqingzhang@sjtu.edu.cn

currently incurable diseases. However, mRNA's inherent instability and electronegativity often lead to degradation by nucleases and low transfection efficiency^{15,16}, necessitating the development of safe and effective nucleic acid delivery systems. The commercialization of ONPATTRO® (Patisiran) and two COVID-19 mRNA vaccines, COMIRNATY and SPIKEVAX, has highlighted the vast potential of lipid nanoparticles (LNPs) in disease prevention and treatment^{17–20}. However, these drugs or vaccines are primarily effective for liver targeting via intravenous injection or for provoking systemic immune response through intramuscular injection, with both exhibiting low pulmonary accessibility. It is reported that only about 20% of drugs reach the lungs after intravenous administration²¹. While oral administration is considered the safest and most convenient method, it poses challenges such as drug absorption and degradation in the acidic environment of the gastrointestinal tract, microbial interference, and a first-pass effect.

Inhaled administration offers many advantages, including maximal drug deposition in the lungs, improving compliance, promoting rapid drug absorption, avoiding first-pass metabolism, and minimizing systemic exposure^{22–25}. Therefore, pulmonary administration is considered an ideal route for treating respiratory diseases. A successful inhaled nucleic acid delivery system must endure the shear force damage during nebulization, evade mucociliary clearance, escape macrophage phagocytosis, and ensure efficient cytoplasmic transport and protein translation^{26,27}. Currently, inhaled LNP-mRNA drugs from companies like Arcturus (ARCT-032), Vertex Pharmaceuticals (VX-522) and Recode Therapeutics (RCT1100) are undergoing clinical trials for treating cystic fibrosis (CF) and primary ciliary dyskinesia (PCD)²⁸, but no inhaled LNP-mRNA candidate drug has successfully completed clinical trials to date. There is an urgent need to develop an inhaled LNP (iLNP) delivery system with translational potential, and an easy-to-use screening method is still being explored.

Herein, we present the “LOOP” platform, a four-step workflow to obtain LNPs with superior shear force resistance and robust luciferase expression, without the need for extensive screening. Firstly, we utilized microfluidics technology to prepare a range of LNPs with adjustable molar ratios of ionizable lipid, cholesterol, helper lipid, and PEG-lipid to achieve LNP with optimal shear force resistance. Secondly, we dialyzed the LNPs against buffers with different compositions and pH values. Thirdly, excipients such as alcohols and nonionic surfactants were introduced into the nebulization buffer to enhance the stability against shear force damage. Lastly, we adjusted lipid molar ratios based on the current dialysis buffer and nebulization buffer, investigating the “lipid composition-activity” relationship. Notably, this “LOOP” approach also demonstrated its versatility in enhancing the stability of LNPs containing ALC0315, a commercially available ionizable lipid used in the COMIRNATY COVID-19 vaccine.

Interleukin-11 (IL-11) has previously been recognized as a potential therapeutic target for IPF²⁹. Full-length antibodies hold significant therapeutic promise due to their unparalleled specificity, high affinity towards antigens, and extended in vivo half-life. However, considering that proteins are prone to aggregation during nebulization due to stress factors and that intravenously injected antibodies are easy to reach non-target organs, we innovatively developed an mRNA-mediated antibody inhalation therapy, which could theoretically mitigate potential off-target effects associated with siRNA targeting IL-11 mRNA. This therapy increases the stability of drugs during nebulization while achieving sustained protein expression, thereby exerting enhanced anti-fibrotic therapeutic effects. In this research, we encapsulated mRNA-encoding IL-11 single-chain fragment variable (scFv mRNA) in a “LOOP”-optimized LNP, termed iLNP-HP08^{LOOP}, to create scFv@iLNP-HP08^{LOOP} (Fig. 1). scFv offers several advantages, including modular design flexibility, low molecular weight, enhanced permeability, and minimal immunogenicity, facilitating the development of bispecific antibodies through precise structural design. When paired with delivery systems, mRNA-encoded scFv can access cryptic

epitopes and intracellular targets, offering solutions for challenging targets while enhancing targeted delivery to specific tissues or cells, thereby minimizing adverse effects^{30–32}. In a mouse model of bleomycin-induced pulmonary fibrosis, both intravenously injected IL-11 scFv and inhaled scFv@iLNP-HP08^{LOOP} significantly inhibited fibroblast activation and extracellular matrix (ECM) production, with the inhaled scFv@iLNP-HP08^{LOOP} exhibiting a more prominent therapeutic effect. Pulmonary function test revealed that inhaled scFv@iLNP-HP08^{LOOP} significantly improved all pulmonary function parameters in fibrotic mice. Moreover, the “LOOP” approach presents a versatile platform for developing other inhaled protein replacement therapies based on mRNA, offering promise for treatments in preventing and managing IPF-incorporated ILDs as well as other respiratory diseases.

Results

“LOOP”-based iLNP screening for nebulized mRNA delivery

In our prior research, we reported the chemical structure and synthesis process of an ionizable lipid compound, AA3-DLin. We validated its cellular biocompatibility and efficacy in mediating protein expression through intramuscular injection in vivo³³. Utilizing the “LOOP” workflow (Fig. 2a), we screened iLNP by designing seven formulations with varying molar ratios of ionizable lipid compound AA3-DLin, 1,2-distearoyl-*sn*-glycero-3-phosphocholine (DSPC), cholesterol, and 1,2-dimyristoyl-*rac*-glycero-3-methoxypolyethylene glycol-2000 (DMG-PEG2000), while maintaining fixed nitrogen to phosphorus ratio of 7.3 between AA3-DLin and luciferase mRNA (mLuc) (Fig. 2b, c). The LNPs were prepared using a microfluidic chip, left at room temperature for 20 min, and then dialyzed against phosphate buffer saline (PBS) at pH 7.4 for 6 h. Figure 2d and Supplementary Table 1 show the encapsulation efficiency (EE) of LNPs before and after nebulization using Ribogreen assay, while Fig. 2e, f and Supplementary Table 1 demonstrate the changes in size and polydispersity index (PDI) of LNPs before and after nebulization determined with dynamic light scattering (DLS). The LNPs with the best overall performance were selected for further optimization based on the following principles: 1) minimal changes in EE after nebulization; 2) particle size of LNP after nebulization not changing more than twofold; 3) PDI of LNP before nebulization less than 0.15. Based on these principles, LNP-3 was chosen for the next optimization step in the “LOOP” workflow. Afterward, we investigated the impact of dialysis buffer on the nebulization stability of LNPs. We dialyzed LNP-3 against PBS or 4-(2-Hydroxyethyl)-1-piperazine ethane sulfonic acid (HEPES) at pH 6.0 or 7.4, respectively. We then measured the changes in EE, size, and PDI of LNPs before and after nebulization in detail. The results in Fig. 2g and Supplementary Table 2 revealed that, when using HEPES at pH 6.0 as the dialysis buffer, the changes in EE, particle size, and PDI of LNPs after nebulization were minimal. Therefore, we selected HEPES at pH 6.0 as the optimal dialysis buffer for further experiments.

Subsequently, we conducted a thorough examination of the impact of excipients on the stability of LNPs. Specifically, we studied the effects of two FDA-approved alcohols, ethanol and propylene glycol (inactive ingredients for nebulization), and poloxamer 188 (known for its stabilizing potential in protein formulations) on the aerosol stability of LNPs^{34,35}. We have summarized the administration routes and dosage forms of FDA-approved drugs containing these excipients in Supplementary Table 3. The experimental results shown in Fig. 3a–c indicated that compared to the control group containing only HEPES, the introduction of these three excipients significantly reduced the changes in particle size, PDI, and EE after nebulization. Notably, higher concentrations of excipients led to smaller changes in particle size and PDI, confirming their ability to enhance the colloidal stability of LNPs. We then administered these LNPs to mouse lungs using a vibrating mesh nebulizer at a dose of 45 µg mRNA per three mice. After 6 h, we extracted the major organs and used the IVIS imaging system to assess luciferase expression. As shown in Fig. 3d, e,

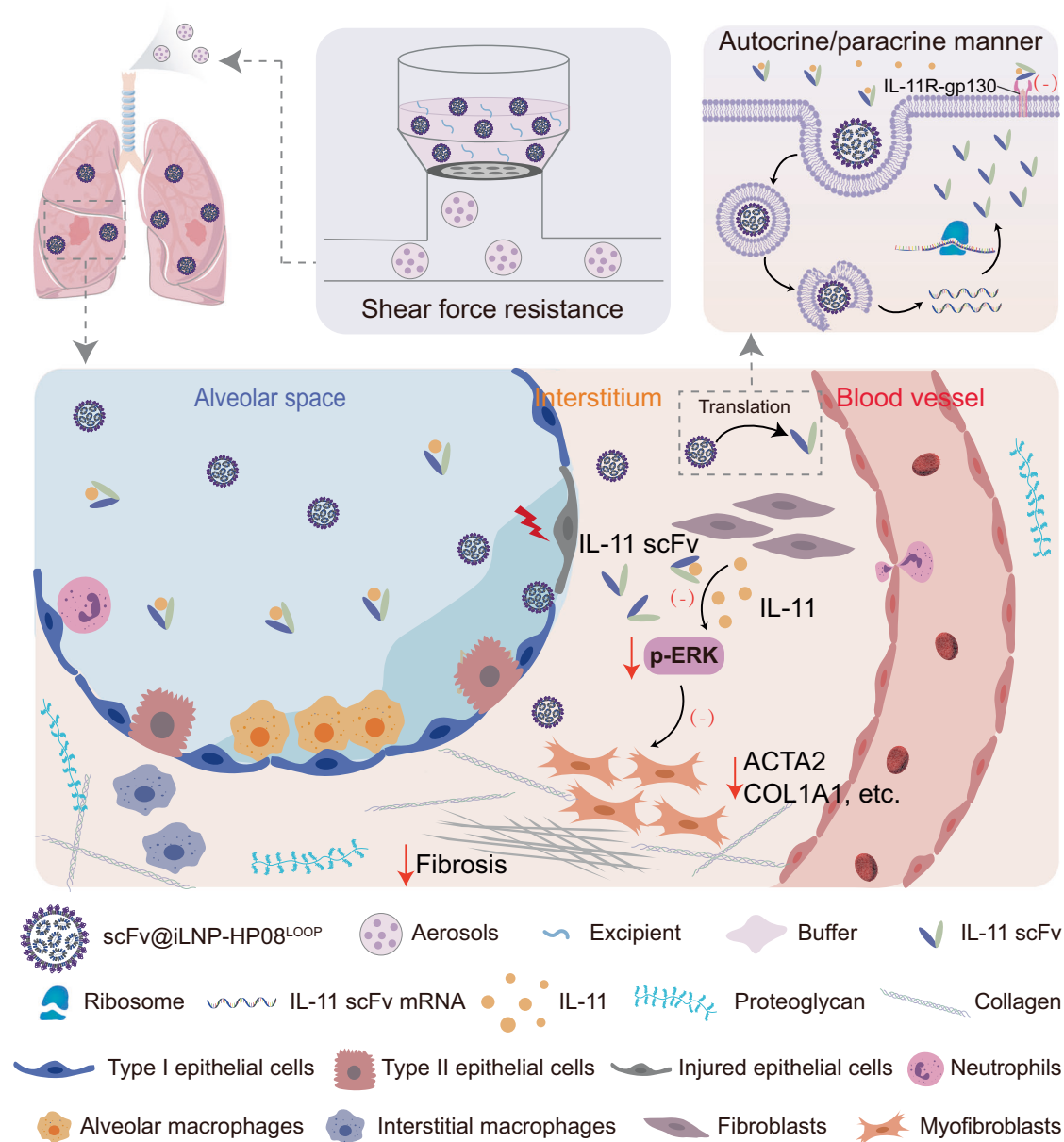


Fig. 1 | Inhaled delivery of scFv@iLNP-HP08^{LOOP} for the treatment of IPF.

“LOOP”-optimized LNP demonstrates improved resistance to shear force damage during nebulization. After inhalation, scFv@iLNP-HP08^{LOOP} enters the pulmonary interstitium and is internalized by diverse array of cell types. The internalized scFv@iLNP-HP08^{LOOP} escapes from endosomes, releases therapeutic scFv mRNA

into cytoplasm, and translates into IL-11 scFv with the aid of ribosomes. The secreted IL-11 scFv binds with IL-11 in an autocrine or paracrine manner and blocks the activation of downstream signaling pathway, which results in a potent anti-fibrotic effect.

an increase in excipient concentration corresponded to an increase in luciferase expression in the lungs, aligning with the enhanced stability of LNPs. No chemiluminescence signal was detected in other organs. Further, a correlation analysis revealed a strong correlation between luciferase expression in the lungs and post-nebulization physiochemical properties of iLNP, including EE, particle size, and PDI, as shown in Supplementary Fig. 1.

Previous research has highlighted that system viscosity and surface tension play crucial roles in determining the properties of aerosols generated through nebulization, including factors like fine particle fraction (FPF) and total output^{36,37}. Specifically, rising viscosity correlates with an increase in FPF, while surface tension affects the sample’s interaction with the gas-liquid interface. Therefore, in this study, we measured the surface tension and viscosity of different nebulization systems. The results showed that the enhanced expression of

luciferase may be related to two factors: reduced surface tension (Fig. 3f) and enhanced solution viscosity (Supplementary Fig. 2). Although the nebulization system containing 12% ethanol showed the highest lung luciferase expression, we observed significant toxicity of LNPs in cytotoxicity experiments within the tested ranges. In contrast, the nebulization system containing 8 mg/mL poloxamer 188 showed good safety and a similar lung luciferase expression level to the system containing 12% ethanol. However, an increase in the concentration of poloxamer 188 to 16 mg/mL and 32 mg/mL exhibited a promoting effect on mouse lung fibroblasts (MLFs) proliferation (Supplementary Fig. 3), which is consistent with the reported literature³⁸. In conclusion, we selected HEPES containing 8 mg/mL poloxamer 188 as the final nebulization buffer. This not only exhibited robust luciferase expression but also ensured the good safety profile of the system, which is consistent with reported results³⁹. We further applied 8 mg/mL

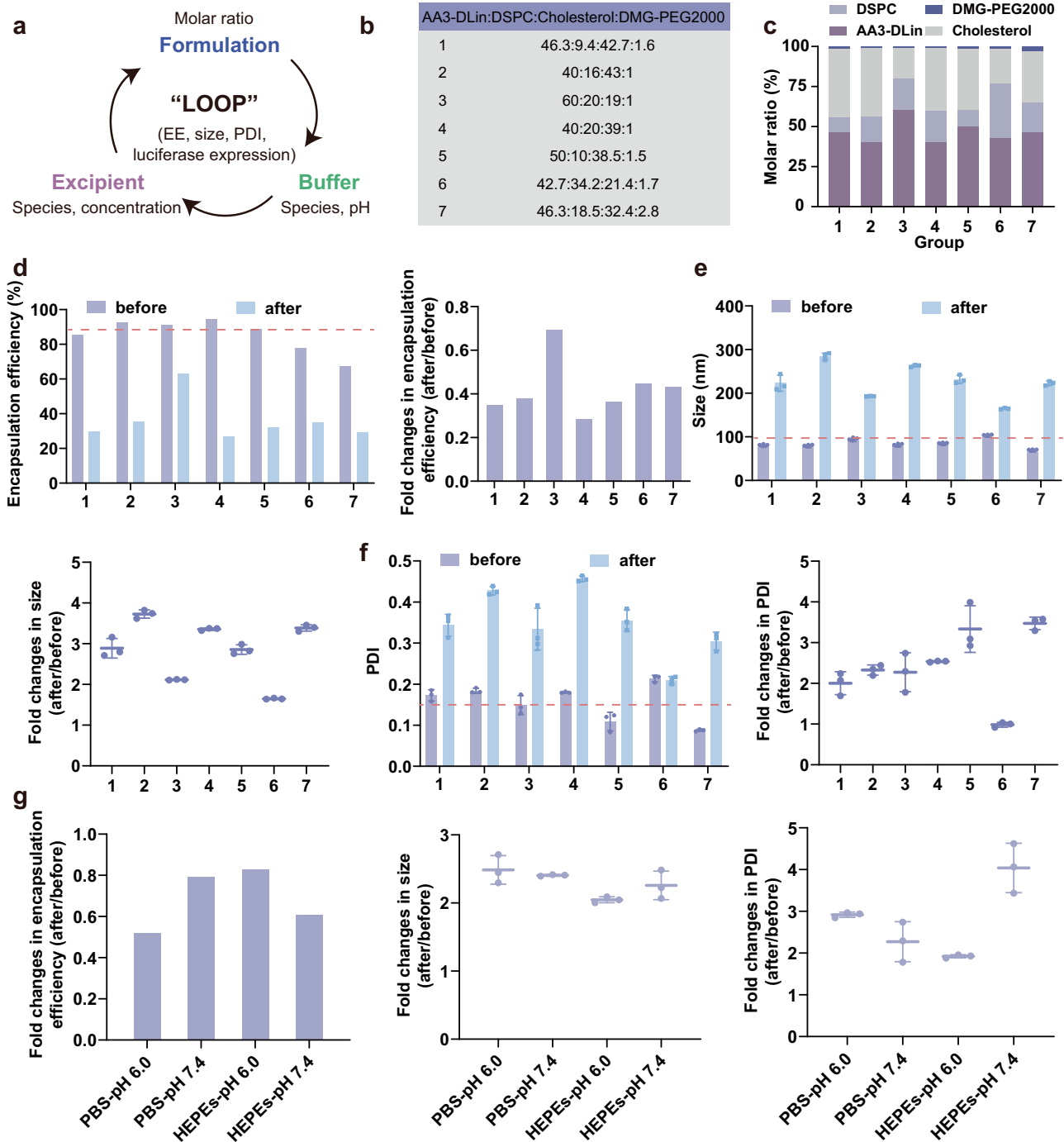


Fig. 2 | Screening of iLNP for nebulized mRNA delivery. **a** A schematic illustration of the screening process for iLNP, utilizing a refined “LOOP” workflow. **b, c** Lipid compositions of the seven tested LNP formulations. Samples were nebulized using a vibrating mesh nebulizer. **d** Determination of EE using a Ribogreen assay. **e, f** Measurements of particle size and PDI using DLS ($n = 3$ biological replicates).

g Nebulization stability analysis for LNPs dialyzed against different buffers. The LNPs were dialyzed against PBS or HEPES at pH 6.0 or 7.4, respectively. The changes in EE, size, and PDI were measured before and after nebulization ($n = 3$ biological replicates). Results are presented as mean \pm s.d. Source data are provided as a Source Data file.

poloxamer 188 to another formulation containing ALC0315 as an ionizable lipid while maintaining the molar ratio of each lipid component unchanged. Supplementary Fig. 4 showed that the introduction of 8 mg/mL poloxamer 188 reduced the changes in size, PDI, and EE after nebulization of LNP and obviously increased luciferase expression in mice lungs by five times compared to nebulized iLNP without the addition of 8 mg/mL poloxamer 188, which confirmed the versatility of the nebulization buffer developed here.

Finally, after establishing the dialysis and nebulization buffer, we studied the relationship between lipid composition and activity by investigating the impact of lipid component variations on luciferase expression in mice lungs. Considering potential variations across different batches of animal experiments, we included a reference formulation with a lipid ratio of 60:20:19:1 in each batch. Comparing the bioluminescence intensity of lung luciferase in various groups to that of the reference group allowed us to acquire relative quantitative

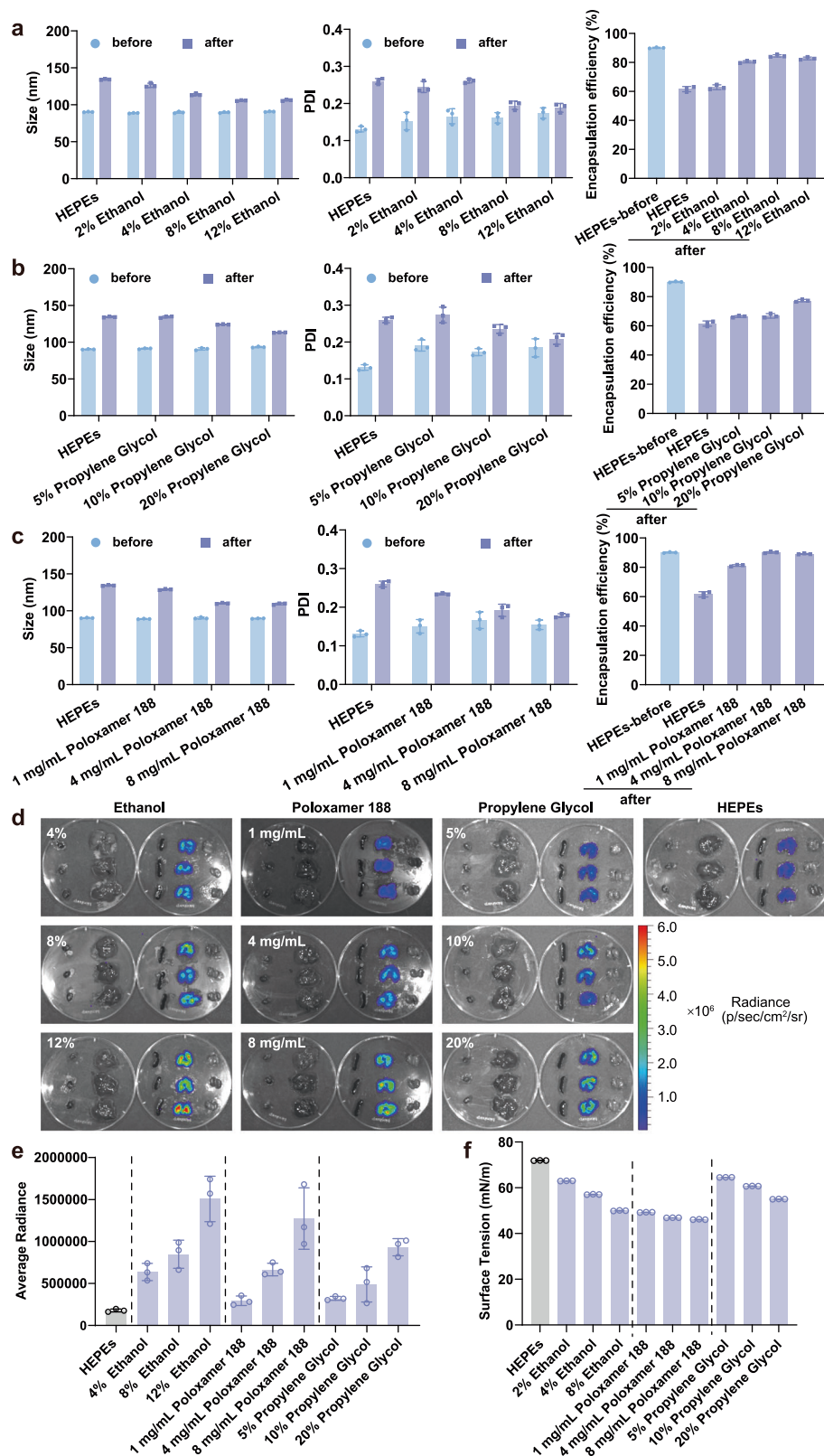


Fig. 3 | Screening of excipients for improved performance of nebulized iLNP. **a–c** Changes in particle size, PDI, and EE of mLuc@iLNP before and after nebulization in the presence of various excipient concentrations ($n = 3$ biological replicates). **d** IVIS imaging of mouse lungs and other organs, including the heart, liver, spleen, and kidney, collected 6 h after nebulization of mLuc@iLNP. Multiple types and concentrations of excipients were tested with mLuc@iLNP, with mLuc@iLNP without excipients serving as the control ($n = 3$ mice per group).

e Quantitative analysis of fluorescence signals in the lungs of mice nebulized with LNPs supplemented with excipients ($n = 3$ biological replicates). **f** Surface tension measurements of nebulization buffers supplemented with varying concentrations of excipients, including ethanol, poloxamer 188, and propylene glycol ($n = 3$ biological replicates). Results are presented as mean \pm s.d. Source data are provided as a Source Data file.

results through normalization. As shown in Supplementary Fig. 5a and 5b, we identified DSPC content and ionizable lipid content as the two most critical factors affecting lung luciferase expression, with DSPC having a more pronounced effect. Specifically, the three worst-performing formulations (60:5:34:1, 58:8:33:1, and 55:10:34:1) had DSPC contents below 10%. Despite increasing ionizable lipid content in the formulations, lung luciferase expression remained low. However, with fixed ionizable lipid content, we observed that increasing DSPC content could significantly enhance the bioluminescence intensity of luciferase in lung tissue. Therefore, we draw our first conclusion: DSPC content in LNP must exceed 10% to achieve desirable luciferase expression. Interestingly, when DSPC content rose to 22%, lung luciferase expression decreased, with cholesterol content dropping to 17%. By measuring particle size changes before and after nebulization, we found that LNP stability decreased when cholesterol content in LNP fell below 19%, with more pronounced particle size changes after nebulization compared to the formulation with a lipid composition of 60:20:19:1 (Supplementary Fig. 5c). Consequently, we arrive at our second conclusion: cholesterol content in LNP must be maintained at above 19% to preserve LNP stability during nebulization process. Similarly, with DSPC content fixed at over 30% and cholesterol at over 19%, we adjusted ionizable lipid content between 43% and 50%, observing no significant changes in luciferase expression. We subsequently established a constant cholesterol content of 19% and a PEG-lipid content of 1%, while varying the ionizable lipid content between 30% and 60%. As illustrated in Supplementary Fig. 5, a consistent decrease in the ionizable lipid content was paralleled by a gradual diminution in the bioluminescence intensity of lung luciferase. Notably, when the ionizable lipid content was below 50%, there was a prominent decline in the expression level of luciferase. Consequently, we arrived at our third conclusion: maintaining a relatively high proportion of ionizable lipid content is essential for ensuring robust expression levels of lung luciferase. Supplementary Fig. 5d and 5e presented the compositions of the three top-performing and the three worst-performing iLNP formulations. Ideal iLNP formulations require careful consideration of these three design principles to achieve optimal lung luciferase expression.

We then prepared five types of mLuc-loaded LNPs, using ALC0315 as the ionizable lipid. As depicted in Supplementary Fig. 6, despite maintaining similar levels of helper lipids in LNP, we observed a remarkable increase in lung luciferase expression efficiency when the ALC0315 content was adjusted to 60%, as opposed to 46.3%. Proceeding further, we kept the ALC0315 molar ratio fixed at 60% while varying the molar ratio of the helper lipid DSPC, specifically at 5%, 10%, 15%, and 20%. The findings revealed that an increase in the proportion of DSPC corresponded to an augmented luciferase expression activity in the lungs, suggesting that the conclusions drawn from Supplementary Fig. 5 are applicable to ALC0315 as well. Ultimately, we selected iLNP-HP08^{LOOP}, with a lipid composition of 60:20:19:1, a dialysis buffer composed of HEPES at pH 6.0, and a nebulization buffer containing 8 mg/mL poloxamer 188, for our subsequent experiments.

Preparation and characterization of iLNP-HP08^{LOOP}

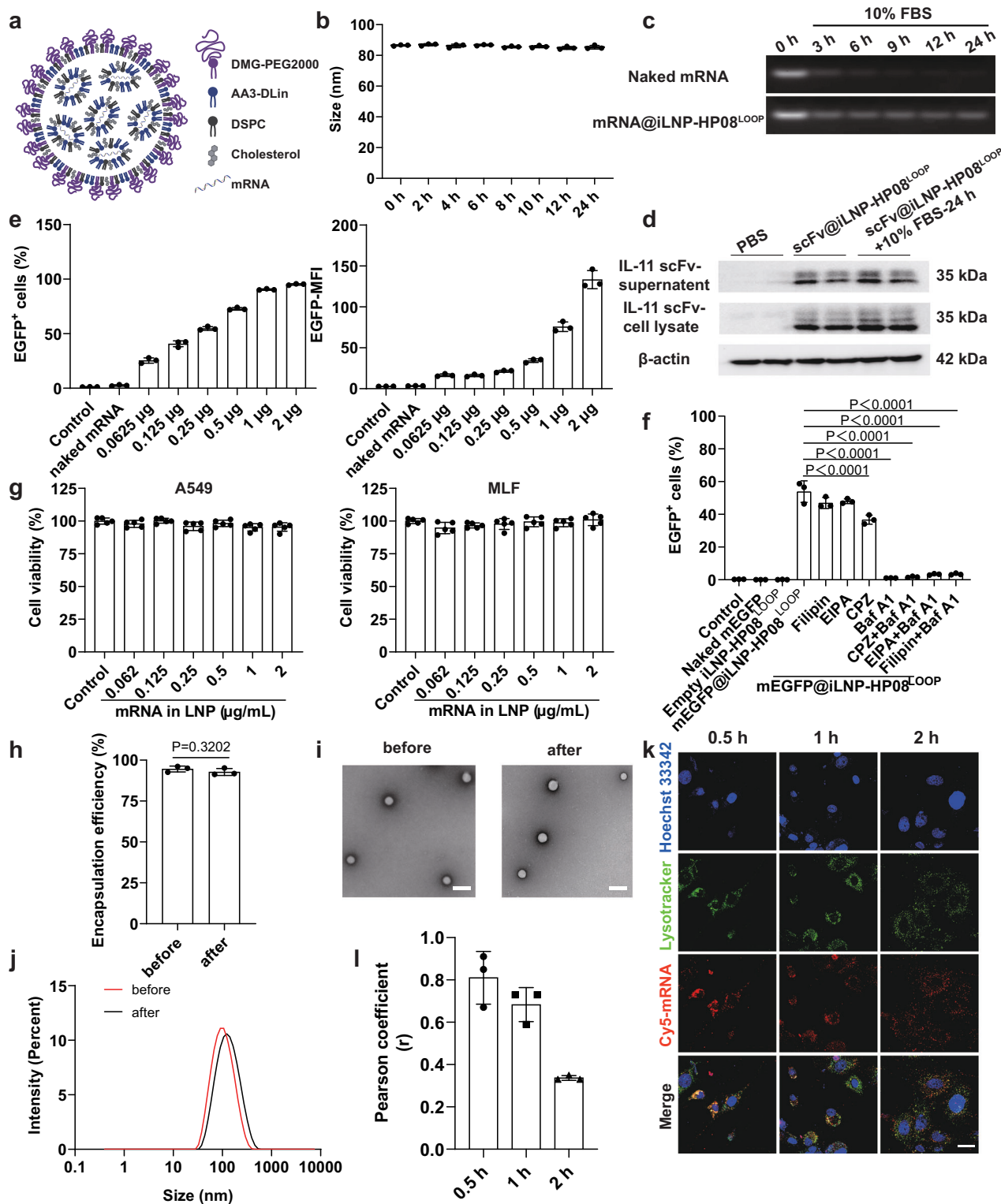
To validate the protective effect of iLNP on mRNA encoding enhanced green fluorescent protein (mEGFP), we used a self-assembly method to prepare mEGFP@iLNP-HP08^{LOOP}, which is composed of mEGFP, AA3-DLin, DSPC, cholesterol, and DMG-PEG2000 (Fig. 4a). Next, we investigated the size stability of iLNP in the presence of serum by incubating mEGFP@iLNP-HP08^{LOOP} with PBS (pH 7.4) containing 10% fetal bovine serum (FBS) for different time periods. DLS results indicated that the size of iLNP-HP08^{LOOP} remained stable within 24 h (Fig. 4b). Additionally, we incubated free mRNA and mRNA@iLNP-HP08^{LOOP} with FBS for various time periods ranging from 0 to 24 h. The results showed that free mRNA was rapidly degraded by FBS, while the mRNA extracted from mRNA@iLNP-HP08^{LOOP} remained structurally intact even after

24 h of incubation with FBS (Fig. 4c). Western blotting analysis demonstrated that FBS did not exert a substantial influence on the mRNA translation efficiency mediated by the LNP (Fig. 4d). The above results suggested that iLNP-HP08^{LOOP} can maintain its stability under physiological conditions. Furthermore, we incubated mEGFP@iLNP-HP08^{LOOP} with MLFs at varying concentrations. Flow cytometry results demonstrated that the transfection efficiency of mEGFP@iLNP-HP08^{LOOP} was dose-dependent (Fig. 4e).

To probe the cellular internalization mechanism of iLNP, we pre-incubated MLFs with various endocytic pathway inhibitors and a proton pump inhibitor before incubating them with mEGFP@iLNP-HP08^{LOOP}. Flow cytometry was then used to measure the transfection efficiency of EGFP. The results in Fig. 4f revealed that pre-treatment with chlorpromazine (CPZ) significantly decreased the percentage of EGFP-positive cells, suggesting that the transfection of mEGFP@iLNP-HP08^{LOOP} is primarily facilitated by clathrin-mediated endocytosis. To ensure the safety of iLNP-HP08^{LOOP}, we selected A549 (type II alveolar epithelial cells) and MLFs as model cells and assessed the safety of iLNP on these cell types. The results of the cell counting kit-8 (CCK8) assay showed no significant cytotoxicity within the tested concentration ranges, even at the highest mEGFP concentration of 2 µg/mL (Fig. 4g). In addition, we investigated the impact of shear force generated during nebulization on the structure of iLNP. Fluorescence assay results showed that the EE of mRNA was not damaged before and after nebulization, with 94.60% before nebulization and 92.77% after nebulization (Fig. 4h). Transmission electron microscope (TEM) images further confirmed that the morphology of iLNP remained spherical after nebulization (Fig. 4i). DLS results also showed no significant changes in the average particle size of iLNP before and after nebulization (Fig. 4j). Moreover, Fig. 4k and Fig. 4l demonstrated that iLNP has the ability to quickly escape from lysosomes, which is essential for the rapid release of mRNA into the cytoplasm and subsequent translation into protein. This finding highlights the potential of iLNP for efficient nucleic acid delivery and expression in cells.

scFv@iLNP-HP08^{LOOP} inhibits MLFs differentiation and migration

We encapsulated mRNA encoding luciferase or IL-11 scFv into iLNP to create mLuc@iLNP-HP08^{LOOP} and scFv@iLNP-HP08^{LOOP}, respectively. We then examined the inhibitory effect of these formulations on fibroblast activation, migration, invasion, and ECM production. The sequence encoding IL-11 scFv was constructed into the pVAX1 plasmid vector, digested overnight with BsaI restriction endonuclease, purified to obtain a linearized plasmid template, and transcribed *in vitro* to obtain IL-11 scFv mRNA (Supplementary Fig. 7). Supplementary Table 4 displayed the amino acid and nucleic acid sequence of IL-11 scFv. Figure 5a shows the structure of IL-11 scFv mRNA, which consists of mRNA sequences encoding heavy chain, light chain, signal peptide, linker peptide, and purification tag. When scFv@iLNP-HP08^{LOOP} was transfected into MLFs, secreted IL-11 scFv was expressed and bound to IL-11 to block the activation of IL-11 signaling pathway. Western blotting was used to detect the expression of IL-11 scFv in cell culture supernatant and cell lysate, and the results showed that the expression of IL-11 scFv was dose-dependent (Fig. 5b and Supplementary Fig. 8). We incubated scFv@iLNP-HP08^{LOOP} with MLFs for 4 h, and samples were then collected at different time points to evaluate the expression of IL-11 scFv. Figure 5c showed that the expression of IL-11 scFv in cell lysate reached the highest level at 72 h, and slightly decreased at 96 h, while the expression in cell culture supernatant continued to accumulate, reaching the highest level at 96 h. This indicated that our IL-11 scFv could be continuously expressed for 3 days, providing a reference for the administration interval in subsequent animal experiments. Figure 5d shows the binding ability of IL-11 to IL-11 scFv, and the calculated EC50 was about 76.18 nM. Figure 5e and Supplementary Fig. 9



demonstrated that IL-11 scFv was successfully expressed in the lungs of mice after inhalation delivery.

Subsequently, we incubated MLFs with either mLuc@iLNP-HP08^{LOOP} or scFv@iLNP-HP08^{LOOP} for 4 h before performing immunofluorescence staining for ACTA2 and COL1A1, which are markers for myofibroblasts and component of the ECM, respectively. Images from a laser scanning confocal microscope (LSCM) showed that scFv@iLNP-HP08^{LOOP} significantly reduced TGF-β1-induced expression of ACTA2 and COL1A1 compared to mLuc@iLNP-HP08^{LOOP} (Fig. 5f–h). Given that fibrosis is also closely related to the migration and invasion of

fibroblasts, we conducted transwell migration experiments to assess the impact of scFv@iLNP-HP08^{LOOP} on MLFs migration (Fig. 5i, j) and invasion (Fig. 5i, k). The MLFs were pre-cultured in a Boyden chamber and incubated separately with mLuc@iLNP-HP08^{LOOP} or scFv@iLNP-HP08^{LOOP}. For the invasion experiment, matrigel was pre-coated in the wells before cell seeding, TGF-β1 was used as a chemical attractant, and a stained solution was used to quantify cell migration. The results in Fig. 5i–k showed that scFv@iLNP-HP08^{LOOP} treatment significantly reduced cell migration and invasion. Subsequently, utilizing IL-11 as the stimulatory factor, we embarked on a detailed exploration of the

Fig. 4 | Characterization of iLNP-HP08^{LOOP}. **a** Schematic representation of mRNA@iLNP-HP08^{LOOP}. **b** Size measurements of mEGFP@iLNP-HP08^{LOOP} incubated in PBS (pH 7.4) containing 10% FBS for 24 h at designated time intervals ($n = 3$ biological replicates). **c** Stability assessment of free mRNA and LNP-encapsulated mRNA in the presence of FBS via electrophoresis. **d** Western blotting analysis investigating the impact of FBS on mRNA transfection efficiency mediated by LNP ($n = 2$ biological replicates). **e** Dose-dependent cell transfection of mEGFP@iLNP-HP08^{LOOP} in MLFs ($n = 3$ biological replicates). **f** Investigation of the endocytic pathway mechanism of mEGFP@iLNP-HP08^{LOOP} in MLFs ($n = 3$ biological replicates). **g** Cell viability study of MLFs and A549 following treatment with different concentrations of mEGFP@iLNP-HP08^{LOOP} ($n = 5$ biological replicates). **h** Determination of EE in mEGFP@iLNP-HP08^{LOOP} before and after nebulization

($n = 3$ biological replicates). **i** Representative TEM images of mEGFP@iLNP-HP08^{LOOP} before and after nebulization. Scale bars, 200 nm. **j** Particle size measurements of mEGFP@iLNP-HP08^{LOOP} before and after nebulization. **k** Representative images showing Cyanine5 (Cy5)-mRNA@iLNP-HP08^{LOOP} escaping from lysosomes. Scale bars, 50 μ m. **l** Calculation of the Pearson correlation coefficient between the fluorescence signals of mRNA and lysosomes at different time points ($n = 3$ biological replicates). Data shown in (c), (d), (i), and (k) are representative of two independent experiments. Results are presented as mean \pm s.d. Statistical significance was analyzed using a two-tailed unpaired Student's *t* test (h) or one-way ANOVA with Tukey test (f). Source data are provided as a Source Data file.

potential function of scFv@iLNP-HP08^{LOOP} in regulating ACTA2 expression, COL1A1 production, and the migratory and invasive capabilities of fibroblasts. As clearly depicted in Supplementary Fig. 10, after incubation with MLF, scFv@iLNP-HP08^{LOOP} significantly mitigated the IL-11-triggered elevation in ACTA2 expression, COL1A1 production, and fibroblast migration and invasion, when compared to the control groups treated with IL-11 + PBS or IL-11+mLuc@iLNP-HP08^{LOOP}. Moreover, western blotting analysis at the cellular level indicated that LNPs containing 1 μ g/mL mRNA obviously reduced the expression level of COL1A1, ACTA2, and p-ERK induced by IL-11 (Supplementary Fig. 11). Overall, these findings suggested that IL-11 scFv effectively inhibited fibroblast activation, ECM deposition, and fibroblast migration into fibrotic lesions.

scFv@iLNP-HP08^{LOOP} inhibits bleomycin-induced pulmonary fibrosis

To prepare for our animal experiments, we first investigated the deposition behavior of fluorescent iLNPs in mice following a single inhalation. Specifically, we created mLuc@iLNP^{Cy5}-HP08^{LOOP} by substituting 20% of the cholesterol (molar ratio) in the iLNP with Cy5-labeled cholesterol. Our findings indicated that upon a single inhalation, these fluorescent LNPs selectively accumulated in the lungs (Supplementary Fig. 12). Subsequently, we utilized flow cytometry to investigate the internalization of iLNP^{Cy5}-HP08^{LOOP} in various cell types following inhalation. We dissociated lung tissues enzymatically and employed antibodies targeting CD31, CD45, EpCAM, and PDGFR α to label endothelial cells, immune cells, epithelial cells, and mesenchymal cells (including fibroblasts), respectively⁴⁰. The flow cytometry analysis revealed that iLNP^{Cy5}-HP08^{LOOP} was primarily internalized by immune cells and mesenchymal cells (Supplementary Fig. 13). Furthermore, we monitored the expression of luciferase in vivo after administering mLuc@iLNP-HP08^{LOOP} through inhalation. Notably, luciferase expression was primarily observed in the mouth, nose, and lungs, with minimal or no expression in other organs (Supplementary Fig. 14). Luciferase expression peaked at 24 h after administration, maintained high levels for 48 h, and gradually declined to nearly undetectable levels by 96 h. These findings provide crucial insights for determining the optimal dosing intervals for our subsequent animal experiments.

To assess the anti-fibrotic potency of scFv@iLNP-HP08^{LOOP}, we established a mouse model of pulmonary fibrosis by administering a single injection of bleomycin intratracheally. To obtain free IL-11 scFv, we transfected IL-11 scFv mRNA into HEK293 cells using PEI, collected the cell culture supernatant three days later, and purified IL-11 scFv using nickel column affinity chromatography. We evaluated its purity using Coomassie Brilliant Blue staining and verified its expression with western blotting (Supplementary Fig. 15). The mice were treated with various administrations every 3 days from day 10 to day 27, including intravenously (i.v.) injected IL-11 scFv, inhaled PBS, inhaled mLuc@iLNP-HP08^{LOOP}, inhaled IL-11 scFv, or inhaled scFv@iLNP-HP08^{LOOP}. The inhaled IL-11 scFv and i.v. injected IL-11 scFv-treated groups received 100 μ g of IL-11 scFv per mouse, while the inhaled scFv@iLNP-

HP08^{LOOP}-treated group received a dosage of 25 μ g IL-11 scFv mRNA per mouse. On day 28 after the bleomycin challenge, the mice were euthanized, and their lungs were collected to evaluate the therapeutic effects (Fig. 6a).

The initial morphological observations revealed that after the bleomycin challenge, the lung tissue was damaged and exhibited increased stiffness. However, when treated with either i.v. injected IL-11 scFv or inhaled scFv@iLNP-HP08^{LOOP}, the damage was significantly reduced, with the latter showing a more pronounced improvement (Fig. 6b). We hypothesized that the rapid degradation of IL-11 scFv post-intravenous injection may be the contributing factor. It's noteworthy that after intravenous injection, free IL-11 scFv was rapidly cleared (Supplementary Fig. 16), whereas scFv@iLNP-HP08^{LOOP} remained detectable in the bronchoalveolar lavage fluid (BALF) for 48 h post-inhalation, maintaining a significantly higher expression level compared to the control group (Supplementary Fig. 17). By weighing the lung tissues from mice in various treatment groups and calculating the organ coefficient, we found that the scFv@iLNP-HP08^{LOOP}-treated group was most effective in reversing the increased lung tissue wet weight induced by bleomycin (Fig. 6c).

Immunofluorescence staining images showed that intratracheal administration of bleomycin triggered excessive myofibroblast differentiation and ECM deposition in the lungs. Fortunately, nebulized scFv@iLNP-HP08^{LOOP} and i.v. injected IL-11 scFv offered significant rescue, with the former exhibiting a more prominent effect (Fig. 6d-f). However, inhaled IL-11 scFv failed to produce the desired therapeutic effect, likely due to the inability of free IL-11 scFv to withstand the shear force generated during nebulization. The determination of hydroxyproline content showed that bleomycin increased the hydroxyproline content in wet lung tissues to 337.3 μ g/lung, whereas scFv@iLNP-HP08^{LOOP} treatment significantly reduced it to 223.3 μ g/lung (Fig. 6g). Consistent with the immunofluorescence results, western blotting analysis showed that inhalation of scFv@iLNP-HP08^{LOOP} greatly suppressed the expression of ACTA2, fibronectin, COL1A1, and IL-11 induced by bleomycin, compared to PBS and mLuc@iLNP-HP08^{LOOP}-treated fibrosis mice (Fig. 6h).

Histological evaluation and signaling pathway analysis

We further conducted histological analysis of lung tissues collected from mice treated with different interventions to investigate the in vivo antifibrotic effects. Through H&E staining, we found that intravenous injection of IL-11 scFv and inhaled scFv@iLNP-HP08^{LOOP} significantly alleviated structural abnormalities (scar formation) caused by normal alveolar tissue injury and abnormal repair after bleomycin challenge. Notably, scFv@iLNP-HP08^{LOOP} exhibited the most prominent inhibitory effect on thickening alveolar septum (Fig. 7a, b). In addition, Masson staining and picrosirius red staining results further demonstrated that scFv@iLNP-HP08^{LOOP} significantly inhibited the production of collagen fibers in the lung interstitium induced by bleomycin (Fig. 7c, d). Previous studies have shown that IL-11 mainly activates the ERK signaling pathway, which in turn triggers fibroblast

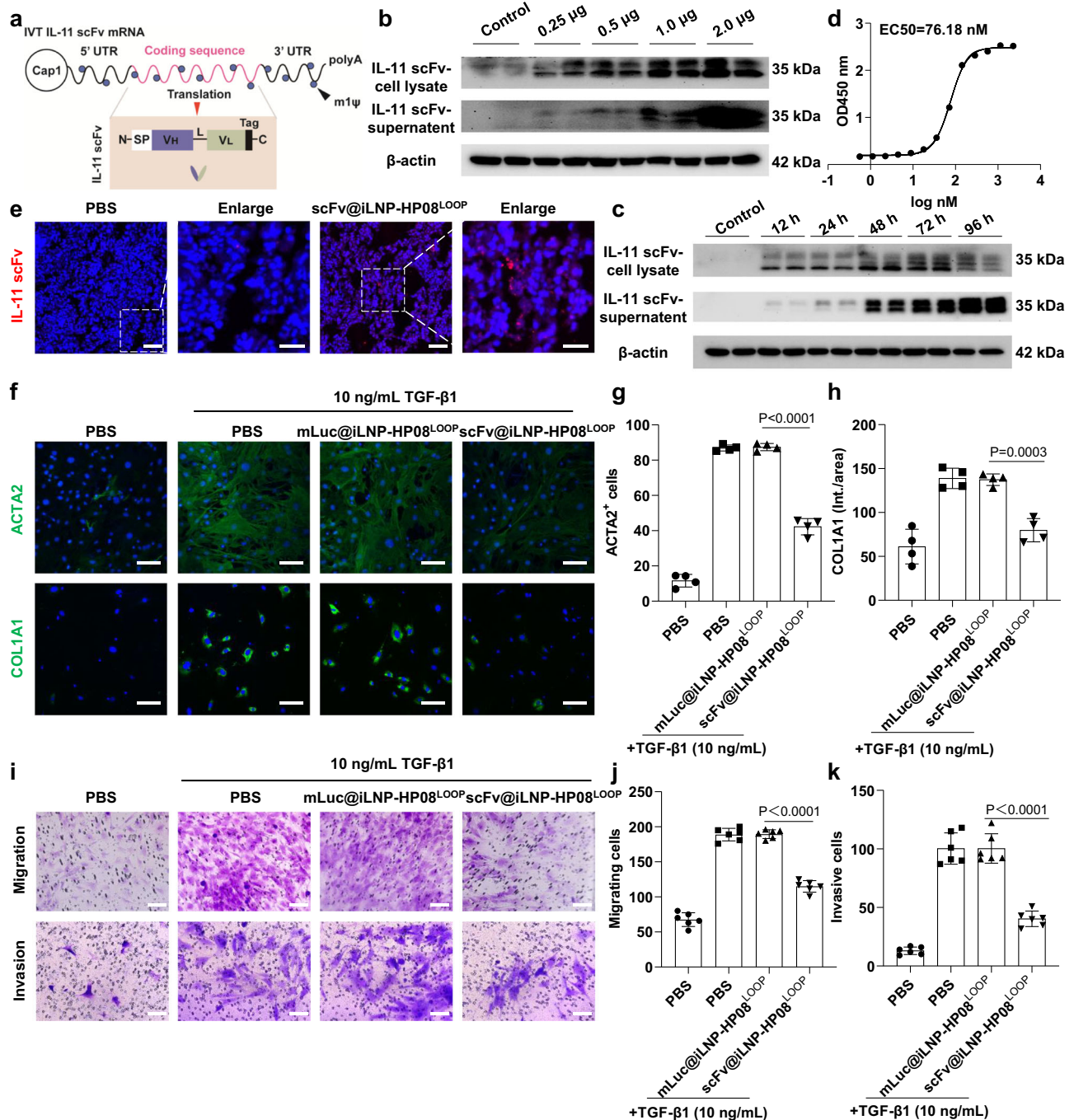


Fig. 5 | The inhibitory effects of scFv@iLNP-HP08^{LOOP} on MLFs differentiation and migration. **a** Schematic representation of the IL-11 scFv mRNA structure. **b** Western blotting analysis of IL-11 scFv in supernatants and lysates from MLFs transfected with different doses of scFv@iLNP-HP08^{LOOP} ($n = 2$ biological replicates). **c** Time-dependent expression of IL-11 scFv in MLFs transfected with a fixed dose of scFv@iLNP-HP08^{LOOP} ($n = 2$ biological replicates). **d** Binding assay between IL-11 and IL-11 scFv ($n = 2$ biological replicates). **e** In vivo translation of IL-11 scFv. Scale bars, 25 μm (left), 10 μm (right). Data are representative of three independent experiments. **f–h** Representative immunofluorescence images of ACTA2 and

COL1A1 in MLFs treated with TGF- β 1 (10 ng/mL) for 24 h in the presence of PBS, mLuc@iLNP-HP08^{LOOP} or scFv@iLNP-HP08^{LOOP} ($n = 4$ biological replicates). MLFs treated with PBS only were used as a negative control. Scale bars, 100 μm . **i–k** Migration and invasion abilities of MLFs treated with PBS, PBS + TGF- β 1, mLuc@iLNP-HP08^{LOOP} + TGF- β 1, or scFv@iLNP-HP08^{LOOP} + TGF- β 1 ($n = 3$ biological replicates). Cells from two non-overlapping fields per membrane were counted. Scale bars, 100 μm . Results are presented as mean \pm s.d. Statistical significance was analyzed using a one-way ANOVA with Tukey test (**g**, **h**, **j**, and **k**). Source data are provided as a Source Data file.

activation and ECM production. Therefore, we used western blotting to detect the activation status of the ERK and STAT3 signaling pathways. The results revealed that, consistent with previous research findings, treatment with scFv@iLNP-HP08^{LOOP} could inhibit the activation of the phosphorylated ERK signaling pathway downstream of IL-11, but STAT signaling pathway remained elevated (Fig. 7e).

Inhaled scFv@iLNP-HP08^{LOOP} treatment improves pulmonary function

Finally, we employed the forced oscillation technique to explore the clinical potential of scFv@iLNP-HP08^{LOOP} in improving pulmonary function. At the end of the experimental period (day 28), pulmonary function test was performed on bleomycin-induced fibrosis mice and

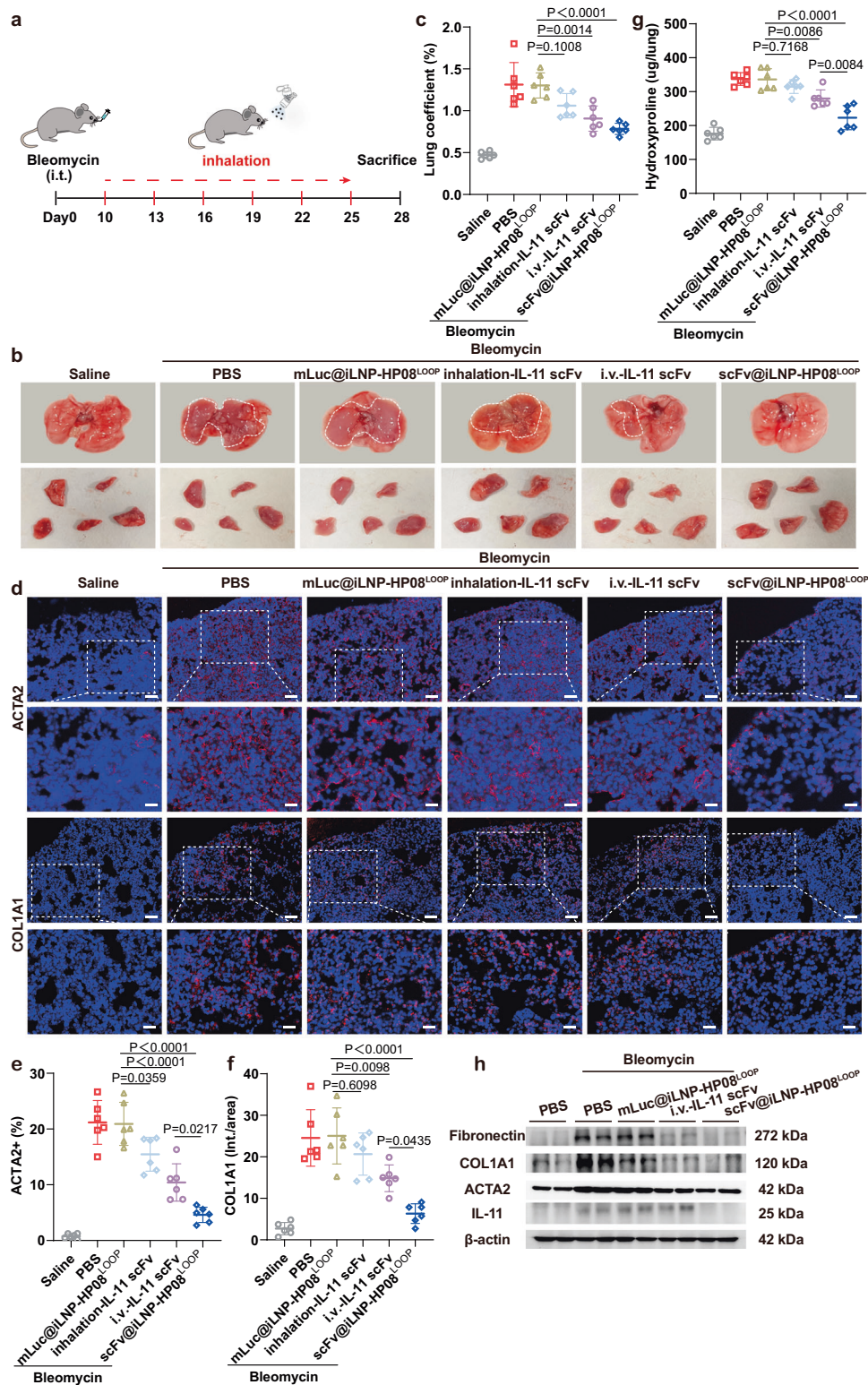


Fig. 6 | Inhaled scFv@iLNP-HP08^{LOOP} inhibits bleomycin-induced pulmonary fibrosis. **a** Experimental design of the animal study. **b** Representative images of mouse lung tissues treated with saline, bleomycin+inhaled PBS, bleomycin+inhaled mLuc@iLNP-HP08^{LOOP}, bleomycin+inhaled IL-11 scFv, bleomycin+i.v. injected IL-11 scFv, and bleomycin+inhaled scFv@iLNP-HP08^{LOOP}. **c** The calculated lung coefficient of mice treated with saline, bleomycin+inhaled PBS, bleomycin+inhaled mLuc@iLNP-HP08^{LOOP}, bleomycin+inhaled IL-11 scFv, bleomycin+i.v. injected IL-11 scFv, and bleomycin+inhaled scFv@iLNP-HP08^{LOOP} ($n = 6$ mice per group). **d–f** Representative immunofluorescence images and quantitative analysis of

COL1A1 and ACTA2 in lung sections from mice treated with saline, bleomycin+inhaled PBS, bleomycin+inhaled mLuc@iLNP-HP08^{LOOP}, bleomycin+inhaled IL-11 scFv, bleomycin+i.v. injected IL-11 scFv, and bleomycin+inhaled scFv@iLNP-HP08^{LOOP} ($n = 6$ mice per group). Scale bars, 100 μ m (upper), 50 μ m (lower). **g** The hydroxyproline content in mouse lung tissues ($n = 6$ mice per group). **h** Western blotting analysis of fibronectin, COL1A1, ACTA2, and IL-11 in mouse lung tissues ($n = 2$ mice per group). Results are presented as mean \pm s.d. Statistical significance was analyzed using a one-way ANOVA with Tukey test (**c**, **e**, **f**, and **g**). Source data are provided as a Source Data file.

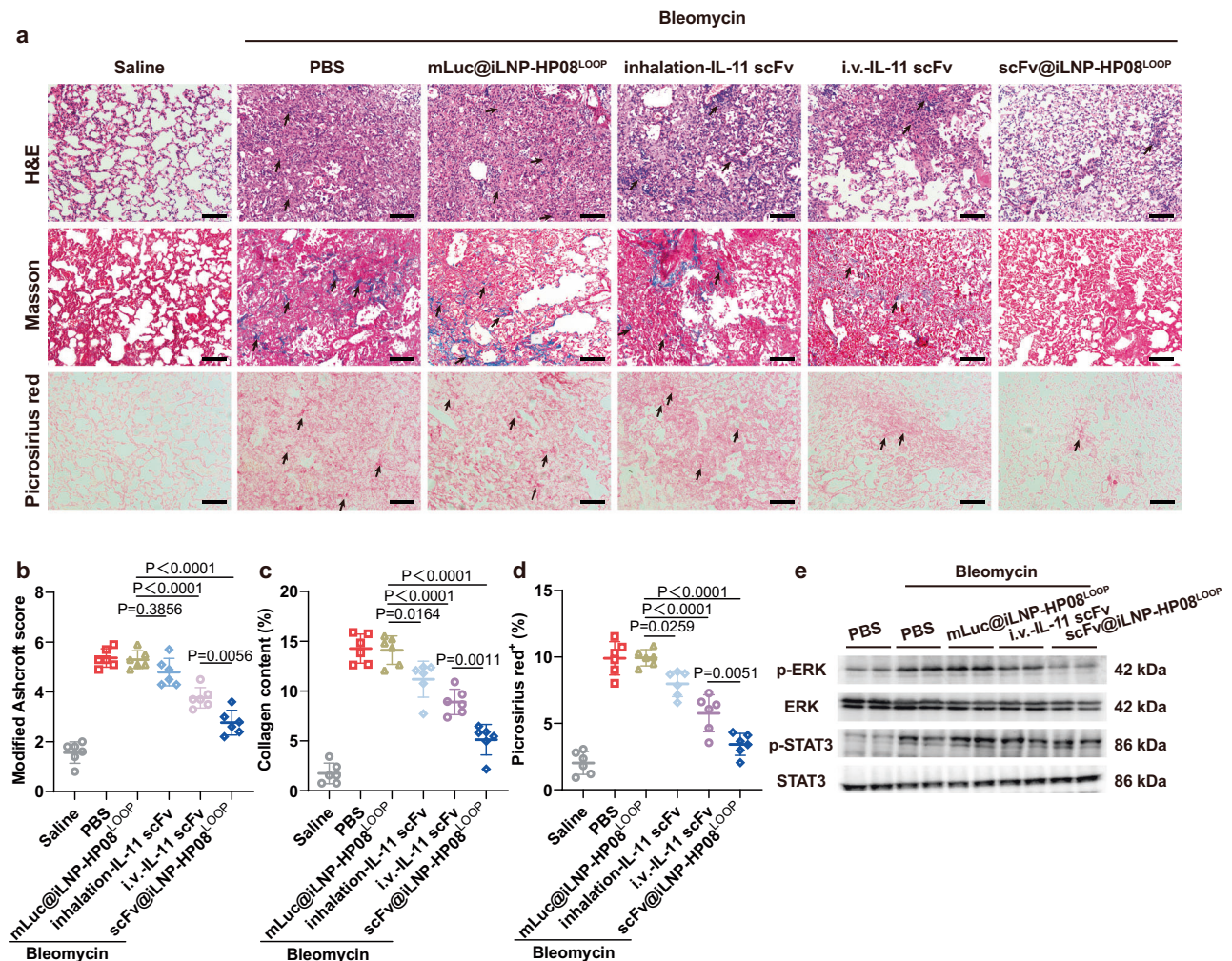


Fig. 7 | Histological evaluation and signaling pathway analysis. a–d Histological staining analysis of mouse lung tissue sections treated with saline, bleomycin +inhaled PBS, bleomycin+inhaled mLuc@iLNP-HP08^{LOOP}, bleomycin+inhaled IL-11 scFv, bleomycin+i.v. injected IL-11 scFv, and bleomycin+inhaled scFv@iLNP-HP08^{LOOP}, including H&E staining, Masson's trichrome staining [collagen (blue), muscle fibers and erythrocytes (red), and nuclei (black-purple)], and picrosirius red

staining (collagen types I and III) (red) ($n = 6$ mice per group). Scale bars, 50 μ m. **e** Western blotting analysis of IL-11 downstream signaling pathways ($n = 2$ mice per group). Results are presented as mean \pm s.d. Statistical significance was analyzed using a one-way ANOVA with Tukey test (**b–d**). Source data are provided as a Source Data file.

healthy mice to evaluate the restorative effect of scFv@iLNP-HP08^{LOOP} on lung function. After bleomycin exposure, respiratory resistance (Rrs) and elastance (Ers) increased significantly, reflecting the impaired constriction and elastic stiffness of the respiratory system including peripheral and conducting airways, chest wall, and parenchyma. Notably, inhaled scFv@iLNP-HP08^{LOOP} treatment significantly improved these parameters in bleomycin-damaged lungs (Fig. 8a, b). In addition, compared to the healthy control group, inspiratory capacity (IC), compliance (Cr_s), forced vital capacity (FVC), static compliance (Cst) and forced expiratory volume at 0.2 s (FEV_{0.2}) were all significantly reduced after bleomycin injury. Expectedly, inhaled scFv@iLNP-HP08^{LOOP} treatment significantly restored all these parameters, particularly IC, Cr_s, FVC, and Cst (Fig. 8c–g). The pressure-volume loop (PV-loop) showed a characteristic downward shift after bleomycin treatment, indicating increased intrinsic elasticity of the lungs, which was significantly improved by inhaled scFv@iLNP-HP08^{LOOP} (Fig. 8h).

In vivo safety evaluation

We conducted an investigation to assess the possible systemic toxicity of inhaled scFv@iLNP-HP08^{LOOP} in mice with bleomycin-induced

pulmonary fibrosis. The mice were sacrificed 3 days after the final inhalation, and their hearts, livers, spleens, kidneys, and blood were collected to evaluate the safety profile of scFv@iLNP-HP08^{LOOP}. As depicted in Supplementary Fig. 18, there were no significant differences in organ coefficients between healthy control group and fibrotic mice treated with inhaled scFv@iLNP-HP08^{LOOP}. Additionally, representative H&E staining images of major organs indicated that inhaled scFv@iLNP-HP08^{LOOP} did not cause any apparent adverse effects (Supplementary Fig. 19a). To further examine the safety profile, we conducted biochemical tests and observed no notable differences between healthy controls and fibrosis mice treated with various treatments, including inhaled PBS, inhaled mLuc@iLNP-HP08^{LOOP}, inhaled IL-11 scFv, intravenously injected IL-11 scFv, and inhaled scFv@iLNP-HP08^{LOOP}, in terms of parameters such as creatinine, urea nitrogen, alanine aminotransferase, aspartate aminotransferase, white blood cell count, red blood cell count, hemoglobin, and lymphocyte (W-SCC) levels (Supplementary Fig. 19b–i). These results suggested that inhaled scFv@iLNP-HP08^{LOOP} did not trigger any side effects in the other organs of mice.

To assess the potential impact of LNP and scFv mRNA on lung function, we performed a pulmonary function test on healthy mice

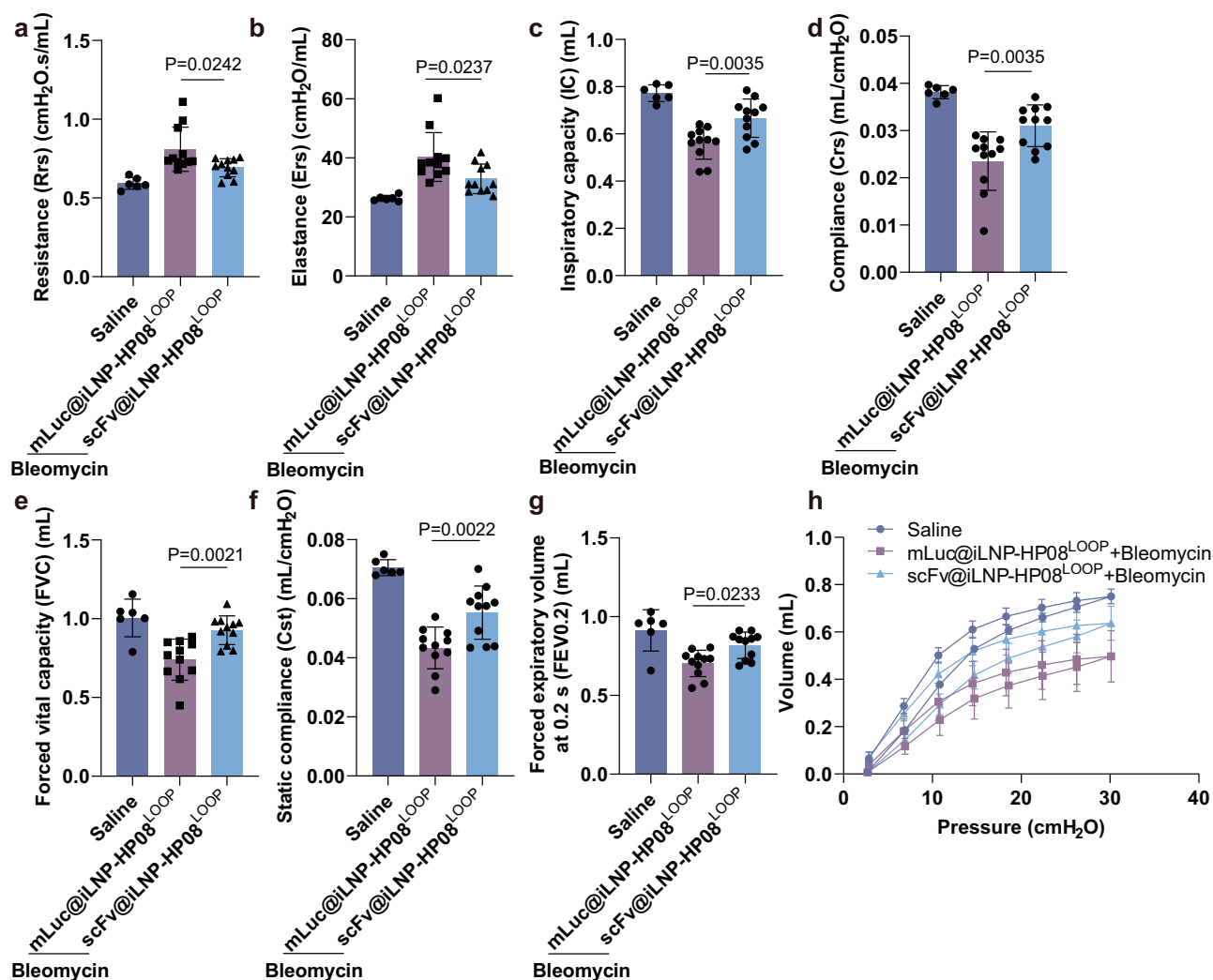


Fig. 8 | Inhaled scFv@iLNP-HP08^{LOOP} restores pulmonary function in the mouse model of bleomycin-induced pulmonary fibrosis. a–g Measurements of pulmonary function parameters, including Rrs (a), Ers (b), IC (c), Crs (d), FVC (e), Cst (f), and FEV_{0.2} (g) ($n = 6$ mice for PBS-treated group and $n = 11$ mice for mLuc@iLNP-HP08^{LOOP}- or scFv@iLNP-HP08^{LOOP}-treated group). **h** Measurements of PV-

loop ($n = 6$ mice for PBS-treated group and $n = 11$ mice for mLuc@iLNP-HP08^{LOOP}- or scFv@iLNP-HP08^{LOOP}-treated group). Results are presented as mean \pm s.d. Significant differences were assessed using a one-way ANOVA with Tukey test (a–g). Source data are provided as a Source Data file.

that were treated with inhaled PBS, inhaled iLNP-HP08^{LOOP}, or scFv@iLNP-HP08^{LOOP}, respectively. As depicted in Supplementary Fig. 20, the inhalation of both iLNP-HP08^{LOOP} and scFv@iLNP-HP08^{LOOP} did not result in any significant alterations in various lung function parameters in mice, indicating that neither LNP nor mRNA caused any adverse effects on lung function. To further evaluate the immunogenicity of LNP and mRNA, we employed ELISA to quantify the levels of inflammatory cytokines, including IL-1 β , IL-6, IFN- γ , and total protein in the BALF of mice. As evident from Supplementary Fig. 21, compared to the control group receiving inhaled PBS, the inhalation of iLNP-HP08^{LOOP} or scFv@iLNP-HP08^{LOOP} did not significantly increase the levels of these inflammatory cytokines or total protein in the BALF. Besides, the BALF inflammatory cytokine levels were not changed at shorter time points such as 6 h or 24 h after a single inhalation of PBS, iLNP-HP08^{LOOP} or scFv@iLNP-HP08^{LOOP} (Supplementary Fig. 22). These findings underscore the excellent safety profiles exhibited by both LNP and IL-11 scFv mRNA utilized in this study.

Discussion

Chronic respiratory diseases (CRDs), encompassing chronic obstructive pulmonary disease, chronic bronchitis, and

bronchiectasis, are significant health issues causing significant losses in life expectancy, livelihoods, health systems, communities, economies, and societies⁴¹. Currently, the treatment options for CRDs are limited to antibiotics, glucocorticoids, and bronchodilators^{42–44}. However, therapeutic antibodies, a targeted therapy derived from natural proteins with comprehensive characterization in terms of toxicity, pharmacodynamics, and pharmacokinetics, have shown promising results in respiratory medicine⁴⁵. Dozens of therapeutic antibodies have been approved for use in the respiratory system. While the standard administration route for therapeutic antibodies is parenteral, typically via intravenous injection, this method limits drug efficacy and poses the risk of systemic toxicity, as only a small fraction reaches the lungs. Inhalation administration provides a more effective alternative, as it maximizes drug enrichment in the lungs, offering benefits such as rapid onset of action, repeated administration, and reduced systemic exposure. For instance, Dornase alfa inhalation has been shown to reduce sputum viscosity and improve CF⁴⁶. Unfortunately, due to their protein nature, antibodies are highly susceptible to thermal inactivation and potential anti-drug-antibody induction, which may negate therapeutic effects^{35,47}.

Currently, only a limited number of inhaled therapeutic antibodies have been approved for use.

mRNA-based protein replacement therapy stands out in preventing infectious diseases like COVID-19 and treating various clinical indications. Its modular design simplifies the research and development cycle, enabling flexibility in treating both rare and common diseases. This therapy facilitates protein expression without nuclear entry, minimizing cellular barriers. Nevertheless, mRNA's immunogenicity, susceptibility to enzymatic degradation, and poor stability during nebulization pose challenges. mRNA vaccines differ by requiring minimal protein expression and activating the immune system through cells and antibodies. For mRNA therapy to reach therapeutic thresholds, protein levels may need to be increased up to 1000 times⁴⁸. Therefore, it is crucial to develop inhalable nucleic acid delivery vectors for efficient lung tissue protein expression. Ideal inhaled vectors should possess: 1) shear force resistance; 2) mucus penetration; 3) high cell transfection efficiency; and 4) cytoplasmic protein expression capability. Suberi et al. using end-group modifications and polyethylene glycol to optimize poly(amine-co-ester) polyplexes for efficiently delivering spike protein mRNA to the lung and successfully triggering robust immune responses in the body⁴⁹. Besides, multiple studies highlight LNP as an effective carrier for delivering nucleic acids to the lungs^{50–52}. Jiang et al. successfully prevented LNP aggregation during nebulization by adjusting the buffer and incorporating branched polymeric excipients. However, the results showed that particle size still underwent obvious changes post-nebulization, and there remains a lack of studies investigating the specific structure-activity relationship between LNP composition and pulmonary luciferase expression⁵³. MRT5005 from Translate Bio is the first mRNA candidate to enter clinical trials for CF treatment, yet interim data from phase I/II trials showed no significant lung function improvement⁵⁴. Companies like Arcturus, Vertex Pharmaceuticals, and Recode Therapeutics are also developing mRNA nanomedicines for CF and PCD treatment, currently in clinical trials. Unfortunately, no inhaled product has yet successfully completed clinical verification.

IPF is a fatal fibrotic lung disease with a short median survival time. Its characteristics include epithelial cell injury, increased number of myofibroblasts, and ECM accumulation. IL-11 is a promising target for IPF treatment. Currently, companies like Lasson Therapeutics and Enleofen have developed full-length antibodies targeting IL-11, exhibiting promising results in IPF management. To diversify treatment options, we developed siRNA therapeutics targeting IL-11 mRNA to validate its anti-fibrotic effect *in vivo*²⁹. We encapsulated siRNA in polymer-lipid hybrid nanoparticles, effectively suppressing IL-11 expression in fibroblasts, thereby preventing their activation and ECM deposition, significantly enhancing lung function in mice. These nanoparticles are resilient to shear force during aerosolization and demonstrate mucus penetration both *in vivo* and *in vitro*. However, there are still areas of improvement. Firstly, we employed GO-C14, which is non-degradable *in vivo*. Secondly, the nanoparticle surface was not modified with ligands, potentially leading to off-target effects of siRNA. Future research must address these challenges to optimize IPF treatment.

In this study, we explored the potential of LNP-mediated RNA delivery as a therapeutic strategy for pulmonary fibrosis. LNP stands as a forefront clinical vector for nucleic acid delivery, exhibiting proven efficacy and safety profiles, as evidenced by numerous marketed siRNA therapeutics and COVID-19 vaccines. Through optimizing the LNP nanomedicine via a “LOOP” process, we identified an optimal formulation capable of enduring shear force damage during nebulization. We further refined the LNP dialysis system and determined that using HEPES buffer at pH 6.0 minimized changes in particle size, PDI, and EE before and after nebulization. Additionally, the addition of excipients further reduced these changes, likely due to a decrease in surface tension and an increase in nebulization system viscosity. While the

addition of ethanol exhibited superior stability during nebulization, it exhibited toxicity *in vitro*. Therefore, balancing luciferase expression and clinical translation potential, we chose 8 mg/mL poloxamer 188 as the final nebulization system. Using this inhalable LNP delivery system, we designed an mRNA encoding IL-11 scFv. Compared to full-length antibodies, scFv has a smaller molecular weight and stronger penetration ability. Upon encapsulation by iLNP and inhalation into mouse lungs, the secreted IL-11 scFv binds to IL-11 in an autocrine or paracrine manner, preventing IL-11 from binding to its corresponding receptors due to steric hindrance. Our findings revealed that iLNP encapsulating IL-11 scFv mRNA was efficiently internalized into cells, rapidly escaping from lysosomes, releasing mRNA into the cytoplasm, and continuously expressing IL-11 scFv. In contrast, after intravenous injection, free IL-11 scFv was undetectable in the blood within 3 h. In a bleomycin-induced pulmonary fibrosis mouse model, inhaled scFv@iLNP-HPO8^{LOOP} demonstrated greater efficacy in reducing ACTA2, COL1A1, and hydroxyproline levels compared to inhaled or intravenously injected IL-11 scFv. Histological examinations revealed that scFv@iLNP-HPO8^{LOOP} treatment significantly alleviated bleomycin-induced alveolar septal thickening, restored damaged alveolar architecture, and reduced collagen deposition and parenchymal destruction. Furthermore, inhaled scFv@iLNP-HPO8^{LOOP} also significantly enhanced lung function recovery in bleomycin-induced fibrosis mice. This marks the application of LNP for the delivery of mRNA encoding scFv in treating IPF, offering promising avenues for IPF treatment.

While current research findings offer promising prospects, further investigations are still necessary. Optimizing drug delivery methods, dosage, and frequency is paramount, particularly in chronic diseases like IPF. Establishing the appropriate dosage and administration frequency is vital to maintaining consistent long-term protein expression and averting the development of drug antibodies. Considering the current dosing frequency of full-length antibodies, ranging from every 2–4 weeks or longer, we aim to explore the use of circular RNA in later stages to minimize dosing requirements. Furthermore, we intend to investigate if the mRNA therapeutics we have developed can target pathways inaccessible to systemically administered antibodies and compare their efficacy with commercially available IL-11 full-length antibodies in the future. The ineffectiveness of many drugs in clinical trials might stem from preclinical models' inability to mimic disease characteristics accurately. Hence, evaluating the drug's efficacy in various mouse models of pulmonary fibrosis is essential to assess its potency and clinical translation potential. Respiratory diseases often exhibit complexities, such as multiple inflammatory pathways and intricate molecular mechanisms, suggesting that exploring drug combinations could enhance therapeutic outcomes. Lastly, given the reported mRNA immunogenicity and inflammatory responses triggered by ionized lipids, closely monitoring the long-term safety profile of mRNA-LNP drugs is crucial^{55,56}. Additionally, the immunogenic nature of PEGylated components may provoke the production of IgM and IgG antibodies against PEG, potentially leading to accelerated blood clearance and complement activation-related pseudoallergy^{57,58}. As a result, comprehensive safety assessments in both small and large animals are imperative for guaranteeing the safety of mRNA-LNP drugs.

In summary, our innovative “LOOP” research platform efficiently screens iLNP nanomedicines, helping us pinpoint top-performing formulations. This system streamlines the refinement of diverse LNPs and selects the most promising candidate. The selected formulation promises to be a versatile platform for inhaled nucleic acid delivery, inclusive of mRNA sequences encoding nanobodies, bispecific antibodies, or full-length antibodies. As such, the “LOOP” platform and the inhaled delivery carrier presented here hold immense potential for leveraging inhaled mRNA therapeutics in the prevention and treatment of respiratory diseases.

Methods

Antibodies

The antibodies used in the research are described as follows: anti-ACTA2 (Servicebio, cat. no. GB111364), anti-IL-11 (Proteintech, cat. no. 55169-1-AP), HRP-conjugated goat anti-mouse IgG (Proteintech, cat. no. SA00001-1), HRP-conjugated goat anti-rabbit IgG (Signalway Antibody, cat. no. L3012), anti-COL1A1 (Abcam, cat. no. ab270993), anti-Fibronectin (Servicebio, cat. no. GB112093), anti- β -actin (Proteintech, cat. no. 66009-1-Ig), Alexa Fluor 488-conjugated goat anti-rabbit IgG (Servicebio, cat. no. GB25303), Cy5-conjugated goat anti-rabbit IgG (Servicebio, cat. no. GB27303), anti-ERK1/2 (Cell Signaling Technology, cat. no. 4695), anti-p-ERK1/2 (Santa Cruz Biotechnology, cat. no. sc-81492), anti-STAT3 (Cell Signaling Technology, cat. no. 9139), anti-p-STAT3 (Cell Signaling Technology, cat. no. 9145), PE anti-mouse CD45 Antibody (BioLegend, cat. no. 103105), Brilliant Violet 421™ anti-mouse CD31 Antibody (BioLegend, cat. no. 102423), FITC anti-mouse CD326 (EpCAM) Antibody (BioLegend, cat. no. 118207), PE/Cyanine7 anti-mouse CD140a Antibody (BioLegend, cat. no. 135911).

In vitro synthesis of mRNA encoding secreted IL-11 scFv

IL-11 scFv mRNA was synthesized according to a previously described method⁵⁹. Briefly, the open reading frame of IL-11 scFv, fused with a 6 × His tag, was cloned into the pVAX1 vector, which already included the T7 promoter, a 5′ untranslated region (UTR) with Kozak sequence, a signal peptide, and a 3′ UTR. Overnight digestion of the plasmids with Bsal-HF (NEB) was performed at 37 °C. Subsequently, the linearized templates were purified using the Universal DNA Purification and Recovery Kit (TIANGEN). In vitro transcription was carried out for 3 h at 37 °C, utilizing T7 RNA polymerase (Novoprotein), as directed by the manufacturer's instructions. This reaction was supplemented with CAP GAG (Hongene) and pseudouridine-5′-triphosphate (Ψ TP; Hongene). The resulting in vitro transcribed mRNA was treated with DNase I (Novoprotein) for 15 min to eliminate the template DNA, and further purified using RNA Clean & Concentrator (Zymo Research). Finally, the mRNA concentrations were accurately measured using a NanoDrop spectrophotometer (Thermo Fisher Scientific).

Preparation of LNPs

mRNA encoding luciferase, EGFP, or IL-11 scFv was diluted in sodium acetate buffer (pH 4.6, 25 mM), while AA3-DLin, DSPC, cholesterol, and DMG-PEG2000 were diluted in 100% ethanol. AA3-DLin was synthesized as previously described³³. DSPC, cholesterol, and DMG-PEG2000 were purchased from AVT. The sodium acetate and ethanol phases were then mixed in a microfluidic device (Aitesen) at a flow rate of 3:1. The resulting mixture was dialyzed against PBS or HEPES at pH 7.4 or 6.0 for 6 h using cassettes with molecular weight cutoff of 3500 Da, followed by further concentration using dialysis tubes with molecular weight cutoff of 100 kDa at 1258 × g. Subsequently, the LNPs were nebulized using a vibrating mesh nebulizer (Aerogen® Solo). Both the LNPs and aerosols were collected for DLS measurements and TEM imaging.

LNP stability assessment

To evaluate the stability of mRNA@iLNP-HP08^{LOOP} and naked mRNA in FBS, agarose gel electrophoresis was conducted. Both naked mRNA and mRNA@iLNP-HP08^{LOOP} were incubated with FBS at 37 °C for varying durations (0 h, 3 h, 6 h, 9 h, 12 h, and 24 h). To release the encapsulated mRNA, mRNA@iLNP-HP08^{LOOP} was disrupted using 2% Triton X-100 (v/v). Both the naked and extracted mRNA were loaded onto Gelred-infused 2% agarose gels for electrophoresis, and band visualization was conducted using a ChemiDoc system (Bio-Rad).

To monitor the size changes of LNPs in serum, samples were aliquoted and incubated with PBS containing 10% FBS under shaking conditions at 37 °C. At predetermined time points, DLS was utilized to measure the particle size (Malvern).

Determination of surface tension and viscosity

To investigate the impact of different nebulization systems on pulmonary drug delivery efficiency, solutions containing ethanol, poloxamer 188, or propylene glycol were prepared in varying concentrations, serving as the nebulization systems. The surface tension of these nebulization systems was then measured using a fully automatic surface tensiometer (Kruss, Germany), adopting the Wilhelmy plate method. Concurrently, the viscosity of these nebulization systems was determined using a viscometer (ATAGO, Japan). The entire procedure was rigorously conducted in accordance with the instructions for the relevant instruments.

Isolation and culture of primary MLFs

MLFs were isolated following a previously described protocol. Briefly, 8-week-old male C57BL/6 mice were euthanized, and their lungs were excised and minced. The lung tissues were then digested in serum-free Dulbecco's modified Eagle's medium (DMEM) supplemented with 1 mg/mL collagenase I for 1 h at 37 °C. Following centrifugation at 582 × g for 3 min, the tissue pellet was washed three times with PBS and resuspended in complete DMEM containing 10% FBS. Lung fibroblasts were allowed to explant from the digested tissues for 4 days, and fibroblasts between passages 3 and 5 were used for subsequent cell experiments. To induce the fibroblast-to-myofibroblast transition, fibroblasts were stimulated with 10 ng/mL TGF- β 1 at 37 °C for 24 h.

In vitro cell transfection study

MLFs were seeded at a density of 5 × 10⁴ cells per well in a 24-well plate and allowed to adhere overnight. The following day, MLFs were incubated with either naked mEGFP or mEGFP@iLNP-HP08^{LOOP} at various mRNA concentrations (0.125, 0.25, 0.5, 1, 2, 4 μ g/mL) for 4 h. Following the initial incubation, the cells were further cultured in complete DMEM for an additional 20 h. To evaluate the cell transfection efficiency of both naked mEGFP and mEGFP@iLNP-HP08^{LOOP}, MLFs were detached using 0.25% trypsin-EDTA, washed three times with PBS, and analyzed using flow cytometry. The percentage of EGFP-positive cells and the average fluorescence intensity for EGFP were then calculated.

Cellular uptake mechanism

MLFs were seeded in a 24-well plate at a density of 5 × 10⁴ cells per well and incubated overnight at 37 °C in 5% CO₂ to facilitate adhesion. On the subsequent day, the cells were pretreated for 30 min with various inhibitors such as 10 μ g/mL EIPA, 10 μ g/mL CPZ, 1 μ g/mL filipin, 200 nM Bafilomycin A1, either individually or in combination, to inhibit micropinocytosis, clathrin-mediated endocytosis, caveolae-mediated endocytosis, or lysosomal proton pump. Following pretreatment, the MLFs were incubated with mEGFP@iLNP-HP08^{LOOP} for 4 h and then further cultured in complete DMEM for 20 h. Thereafter, flow cytometry was used to analyze EGFP expression in the MLFs pretreated with the different inhibitors.

Cell viability assay

A549 (a type of alveolar type II epithelial cell) was purchased from Zhong Qiao Xin Zhou Biotechnology Co., Ltd (Shanghai, China) (cat. no. ZQ0003). MLFs or A549 were seeded in a 96-well plate at a density of 1 × 10⁴ cells per well and allowed to adhere overnight. The following day, the cells were incubated with mEGFP@iLNP-HP08^{LOOP} at various concentrations (0.062, 0.125, 0.25, 0.5, 1, 2 μ g/mL) at 37 °C in 5% CO₂. After 24 h, the supernatant was discarded, and a serum-free medium-diluted CCK8 solution was added to each well. The cells were then incubated for 2 h at 37 °C, and the absorbance at 450 nm was determined using a microplate reader (Tecan).

Determination of encapsulation efficiency

The encapsulation efficiency (EE) of mRNA was determined using a Quant-iT™ RiboGreen RNA Assay kit. To measure the content of free

mRNA and total mRNA, iLNP samples were dispersed in 1×TE buffer or 1×TE buffer containing 2% Triton X-100, respectively. rRNA standard was diluted in a series of concentrations with 1×TE buffer. Equal volumes of iLNP samples or rRNA standard were mixed with 1:200 diluted RiboGreen reagents in a clear-bottom black plate and incubated at room temperature for 5 min. The fluorescence intensity of the mixture was then measured at an excitation wavelength of 480 nm and an emission wavelength of 520 nm using a microplate reader. Finally, EE was calculated using the following formula: EE (%) = (fluorescence of total mRNA-fluorescence of free mRNA)/fluorescence of total mRNA × 100%.

Lysosomal escape study

MLFs were cultured overnight on confocal dishes and then incubated with iLNP encapsulating Cy5-labeled mRNA (Cy5-mRNA@iLNP-HP08^{LOOP}). At designated time intervals, the supernatant containing Cy5-mRNA@iLNP-HP08^{LOOP} was discarded, and the MLFs were washed three times with PBS. Subsequently, the cells were incubated with Lyso-Tracker Green (Beyotime) for 30 min. Following three PBS washes, the nuclear DNA was visualized by staining the MLFs with Hoechst 33342 (Beyotime) for 10 min. LSCM was used to capture the lysosomal escape process of the Cy5-mRNA@iLNP-HP08^{LOOP}.

Purification and evaluation of IL-11 scFv

For the purification of IL-11 scFv, mRNA encoding the protein was transfected into HEK293 cells using PEI at a ratio of 5:1 (PEI:mRNA weight ratio). After a three-day incubation period, the supernatant was collected and concentrated using dialysis tubes with a molecular weight cutoff of 10 kDa at 3220 × g. A single-step immobilized metal affinity chromatography process, relying on the binding affinity between the 6×His tag and a nickel column, was then employed to purify the protein. The purity of the IL-11 scFv was assessed using sodium dodecyl sulfate polyacrylamide gel electrophoresis (SDS-PAGE).

To determine the median effective concentration (EC50) of IL-11 scFv and IL-11, 80 ng of IL-11 was added into each well of a 96-well plate and incubated overnight at 4 °C. The next day, 100 μL of purified IL-11 scFv at different concentrations was added into each well and incubated at 37 °C for 2 h. The liquid was then discarded, and 100 μL of His-tag primary antibody was added and incubated for 1 h at 37 °C. Afterwards, a secondary antibody was added and the mixture was incubated for an additional hour at 37 °C. Then, 3, 3',5,5'-Tetramethylbenzidine substrate was added, and the reaction was terminated using 2 M H₂SO₄. The absorbance was measured at 450 nm using a microplate reader (Tecan).

Immunofluorescence staining of ACTA2 and COL1A1

MLFs were seeded onto coverslips and allowed to attach overnight. The following day, the cells were transfected with mLuc@iLNP-HP08^{LOOP} or scFv@iLNP-HP08^{LOOP} for 4 h, and then further incubated in complete medium containing 10% FBS for 20 h. After stimulation with 10 ng/mL TGF-β1 or 20 ng/mL IL-11 for 24 h, the cells were fixed in 4% paraformaldehyde and permeabilized in 0.1% Triton X-100. The cells were then washed three times with PBS and incubated with anti-ACTA2 or anti-COL1A1 primary antibodies, along with Alexa Fluor 488-conjugated secondary antibodies. DAPI was used to visualize the cell nuclei. All images were captured using LSCM (Leica) and quantified with Imaged J software.

Migration and invasion assay

Equal numbers of MLFs were seeded in a 24-well Boyden chamber, either plain or coated with Matrigel, to evaluate their migratory and invasive capabilities, respectively. The next day, the cells were transfected with mLuc@iLNP-HP08^{LOOP} or scFv@iLNP-HP08^{LOOP} for 4 h, followed by incubation in complete medium containing 10% FBS for

20 h. Subsequently, the cells were starved in serum-free medium for 24 h. TGF-β1 (10 ng/mL) or IL-11 (20 ng/mL) was used as a chemoattractant to induce migration or invasion of MLFs from the upper chamber to the lower chamber. After 24 h, the membranes were fixed with 4% paraformaldehyde and washed three times with PBS. The non-migratory cells in the upper chamber were gently removed with cotton swabs. The migrated cells in the lower chamber were stained with crystal violet solution (Service bio) for visualization. The stained cells were then imaged using an upright microscope (Olympus) at 20× magnification. Cells from two non-overlapping fields of each membrane were counted using Image J software.

Animals

Male C57BL/6 mice (between 8 and 10 weeks old) were purchased from Shanghai Lingchang Biotechnology Co., Ltd. and housed in a specific pathogen-free environment (-18–23 °C, 40–60% humidity) on a 12 light/12 dark cycle. Sex was not considered in the study design and analysis as both male and female mice have been used in the published research papers. To induce pulmonary fibrosis, mice were anaesthetized and administered an intratracheal injection of 1.2 U/kg bleomycin sulfate. After ten days, the mice were randomly assigned to six groups and treated with inhaled PBS, inhaled mLuc@iLNP-HP08^{LOOP}, inhaled IL-11 scFv, intravenously injected IL-11 scFv, and inhaled scFv@iLNP-HP08^{LOOP}, administered on days 10, 13, 16, 19, 22, and 25 using a vibrating mesh nebulizer. A sham control group received an intratracheal injection of saline. On day 28, the mice were euthanized, and blood samples along with heart, liver, spleen, lung, and kidney were collected for the evaluation of therapeutic efficacy and safety. All animal experiments were approved by the Institutional Animal Care and Use Committee at Shanghai Jiao Tong University.

Deposition study

To track the deposition of mLuc@iLNP, a modified version (mLuc@iLNP^{Cy5}-HP08^{LOOP}) was created by replacing 20% of the cholesterol with Cy5-labeled cholesterol. Mice were nebulized with mLuc@iLNP^{Cy5}-HP08^{LOOP} using a vibrating mesh nebulizer (Aerogen® Solo). After 6 h, the mice were sacrificed, and their major organs were collected for fluorescence imaging using the IVIS system (PerkinElmer). The lungs were then fixed, dehydrated, and embedded in optimal cutting temperature compound. The lungs were then sliced into 10 μm-thickness sections. Sections were counterstained with DAPI to visualize cell nuclei. LSCM was used for the visualization of mLuc@iLNP^{Cy5}-HP08^{LOOP} deposition within the whole lung, bronchi, and alveoli.

Bioluminescence study

mLuc was encapsulated into iLNPs formulated with four lipids in varying molar ratios. These iLNPs were diluted in nebulization buffers containing different kinds and concentrations of excipients. Mice were then nebulized with these iLNPs using a vibrating mesh nebulizer (Aerogen® Solo). Six hours later, luciferin was injected intraperitoneally at a dose of 0.15 mg/g body weight. After 5 min, the mice were sacrificed, and major organs were excised for bioluminescence imaging using an IVIS system (PerkinElmer).

Analysis of the in vivo cellular uptake of inhaled iLNP^{Cy5}-HP08^{LOOP}

To investigate the cellular uptake of iLNP within various lung cell types following inhalation, we administered iLNP^{Cy5}-HP08^{LOOP} to mice via a vibrating mesh nebulizer. Six hours later, the mice were euthanized, and their lung tissues were excised and enzymatically dissociated in a PBS solution containing collagenase I (201.3 U/mL; Yeason), DNase I (50.3 U/mL; Sigma-Aldrich), collagenase XI (566.1 U/mL; Sigma-Aldrich), and HEPes (0.92 M; Beyotime). The resulting cell suspension was filtered through a 70 μm cell strainer and then treated with a red

blood cell lysis solution. Following centrifugation, the cell pellet was gently resuspended in PBS and labeled with zombie dye at room temperature for 30 min. After centrifugation, the cells were resuspended in a cell staining buffer containing an Fc Receptor Binding Inhibitor to prevent nonspecific antibody binding. Subsequently, the cells were incubated with antibodies specific to CD31, CD45, EpCAM, and PDGFR α for 20 min at 4 °C to identify endothelial cells, immune cells, epithelial cells, and mesenchymal cells, respectively. Finally, flow cytometry was used to quantitatively assess the cellular uptake of iLNP^{Cy5}-HP08^{LOOP} by the diverse lung cell types.

Histological analysis

The mouse lungs were fixed in 4% paraformaldehyde, dehydrated, and embedded in paraffin. Lung tissues were sliced into 5- μ m-thick sections using a rotary microtome (Leica), and the sections were dewaxed to water using xylene and gradient ethanol. The sections were then stained with H&E, Masson's trichrome, and Picrosirius red solutions to evaluate the severity of fibrosis and the content of collagen. An upright microscope was used to photograph the lung sections. For immunofluorescence analysis, sections were dewaxed to water and then incubated with 3% BSA for 30 min to block non-specific binding sites. Sections were then incubated with anti-ACTA2 or anti-COL1A1 antibodies at 4 °C overnight, further incubated with Cy5-labeled secondary antibodies for 1 h at room temperature, and counterstained with DAPI to visualize cell nuclei. LSCM was used to capture images of lung sections from mice treated with different groups. All pictures were then quantified using Image J software.

Hydroxyproline assay

The mouse lung hydroxyproline content was measured using an alkaline hydrolysis kit. Briefly, 30 mg of lung tissue was precisely weighed and hydrolyzed at 100 °C for 20 min. The pH of the resulting hydrolysate was adjusted to between 6.0 and 6.8. After treatment with activated carbon, the mixture was centrifuged at 2465 \times g for 10 min. The supernatant was then collected and incubated with detection agents at 60 °C for 15 min. Finally, a UV spectrophotometer (SHIMADZU) was used to measure the hydroxyproline content by recording the absorbance at 550 nm.

Western blotting analysis

To evaluate the dose-dependent expression of scFv@iLNP-HP08^{LOOP}, MLFs were seeded in a 24-well plate at a density of 5×10^4 cells per well and cultured overnight. The next day, cells were treated with varying concentrations of scFv@iLNP-HP08^{LOOP} for 4 h and then further incubated in complete DMEM for 24 h. For the time-dependent expression analysis, cells were incubated with 1 μ g/mL scFv@iLNP-HP08^{LOOP} for 4 h, followed by incubation in complete medium for 8, 20, 44, 68, and 92 h. The cell supernatants were collected, and the cells were lysed using a lysis buffer containing 1 \times protease and phosphatase inhibitor cocktail. The lysate was centrifuged to remove cell pellet. Similarly, quick-frozen right lung tissues from mice treated with different groups were homogenized in lysis buffer containing 1 \times protease and phosphatase inhibitor cocktail using a tissue homogenizer. The homogenates were centrifuged, and the supernatant was collected.

The total protein concentration in each sample was determined using the BCA protein assay. For western blotting analysis, samples were mixed with loading buffer, separated by SDS-PAGE, and transferred onto a polyvinylidene difluoride membrane. The membrane was blocked with 5% skim milk powder and incubated overnight at 4 °C with primary antibodies. After washing, the membrane was incubated with secondary antibodies for 1 h at room temperature. Electrochemiluminescence chromogenic substrate was added dropwise to visualize the protein bands under a ChemiDoc imaging system (BioRad). The uncropped and unprocessed scans of the blots have been provided in the Source Data file.

Safety evaluation

To assess the potential toxicity of scFv@iLNP-HP08^{LOOP} on other organs, we measured the organ coefficients by weighing the heart, liver, spleen, and kidneys. The organs were then fixed in 4% paraformaldehyde, dehydrated, and embedded in paraffin. Tissue sections of 5 μ m thickness were obtained and stained with H&E solution to evaluate any pathological changes. Blood samples were also collected for analysis of biochemical and hematological indicators.

To further investigate whether iLNP and mRNA can cause immunogenicity in the lungs, we conducted an experiment where healthy mice were treated with inhaled PBS, iLNP-HP08^{LOOP}, or scFv@iLNP-HP08^{LOOP} every three days for a total of six administrations. Three days after the final administration, BALF was collected from each group of mice, and ELISA was used to quantify the levels of inflammatory cytokines, including IL-1 β , IL-6, and IFN- γ .

Pulmonary function test

Following the final drug administration, healthy and fibrotic mice were anaesthetized with pentobarbital via intraperitoneal injection and intubated with a 14-gauge cannula. Pulmonary function was assessed using a FlexiVent system (SCIREQ), where Rrs, Ers, and Crs were determined through a single-frequency forced oscillation maneuver. IC was measured using a deep inflation maneuver, while FVC and FEV0.2 were quantified using a negative pressure forced expiration maneuver. Lastly, Cst was calculated based on the PV-loop.

Statistical analysis

All data are analyzed using the GraphPad Prism software, version 8.2.1, and the results are presented as mean \pm s.d. The two-tailed unpaired Student's *t* test or a one-way ANOVA with Tukey test is used to analyze statistical differences as specified in the figure legends. *P* values below 0.05 are considered statistically significant.

Reporting summary

Further information on research design is available in the Nature Portfolio Reporting Summary linked to this article.

Data availability

The main data supporting the results of this study are available within the paper and its Supplementary Information. Source data are provided in this paper. Any additional raw data are available for research purposes from the corresponding authors upon reasonable request. Source data are provided in this paper.

References

1. Bowman, W. S., Echt, G. A. & Oldham, J. M. Biomarkers in progressive fibrosing interstitial lung disease: optimizing diagnosis, prognosis, and treatment response. *Front. Med.* **8**, 680997 (2021).
2. du Bois, R. M. Strategies for treating idiopathic pulmonary fibrosis. *Nat. Rev. Drug Discov.* **9**, 129–140 (2010).
3. Mei, Q., Liu, Z., Zuo, H., Yang, Z. & Qu, J. Idiopathic pulmonary fibrosis: an update on pathogenesis. *Front. Pharmacol.* **12**, 797292 (2022).
4. Raghu, G., Yang, S. T. Y., Spada, C., Hayes, J. & Pellegrini, C. A. Sole treatment of acid gastroesophageal reflux in idiopathic pulmonary fibrosis—a case series. *Chest* **129**, 794–800 (2006).
5. Iwai, K., Mori, T., Yamada, N., Yamaguchi, M. & Hosoda, Y. Idiopathic pulmonary fibrosis—epidemiologic approaches to occupational exposure. *Am. J. Respir. Crit. Care Med.* **150**, 670–675 (1994).
6. Raghu, G. et al. Long-term treatment with recombinant human pentraxin 2 protein in patients with idiopathic pulmonary fibrosis: an open-label extension study. *Lancet Respir. Med.* **7**, 657–664 (2019).
7. Corboz, M. R. et al. Therapeutic administration of inhaled INS1009, a treprostinil prodrug formulation, inhibits bleomycin-induced

- pulmonary fibrosis in rats. *Pulm. Pharmacol. Ther.* **49**, 95–103 (2018).
8. Demedts, M. et al. High-dose acetylcysteine in idiopathic pulmonary fibrosis. *N. Engl. J. Med.* **353**, 2229–2242 (2005).
 9. mRNA-based therapeutics. Powerful and versatile tools to combat diseases. *Signal Transduct. Target. Ther.* **7**, 1975–2009 (2022).
 10. Sahin, U., Kariko, K. & Tuercci, O. mRNA-based therapeutics—developing a new class of drugs. *Nat. Rev. Drug Discov.* **13**, 759–780 (2014).
 11. Pardi, N., Hogan, M. J., Porter, F. W. & Weissman, D. mRNA vaccines—a new era in vaccinology. *Nat. Rev. Drug Discov.* **17**, 261–279 (2018).
 12. Kim, Y.-K. RNA therapy: current status and future potential. *Chonnam Med. J.* **56**, 87–93 (2020).
 13. Chaudhary, N., Weissman, D. & Whitehead, K. A. mRNA vaccines for infectious diseases: principles, delivery and clinical translation. *Nat. Rev. Drug Discov.* **20**, 817–838 (2021).
 14. Deal, C. E., Carfi, A. & Plante, O. J. Advancements in mRNA encoded antibodies for passive immunotherapy. *Vaccines* **9**, 108 (2021).
 15. Huang, X. et al. The landscape of mRNA nanomedicine. *Nat. Med.* **28**, 2273–2287 (2022).
 16. Kim, Y. et al. The potential of cell-penetrating peptides for mRNA delivery to cancer cells. *Pharmaceutics* **14**, 1271 (2022).
 17. Xu, K. et al. A novel mRNA vaccine, SYS6006, against SARS-CoV-2. *Front Immunol.* **13**, 1051576 (2022).
 18. Hammerschmidt, S. I. et al. Robust induction of neutralizing antibodies against the SARS-CoV-2 Delta variant after homologous Spikevax or heterologous Vaxzevria-Spikevax vaccination. *Eur. J. Immunol.* **52**, 356–359 (2022).
 19. Luxi, N. et al. COVID-19 vaccination in pregnancy, paediatrics, immunocompromised patients, and persons with history of allergy or prior SARS-CoV-2 infection: overview of current recommendations and pre- and post-marketing evidence for vaccine efficacy and safety. *Drug Saf.* **44**, 1247–1269 (2021).
 20. Dong, Y., Siegwart, D. J. & Anderson, D. G. Strategies, design, and chemistry in siRNA delivery systems. *Adv. Drug Deliv. Rev.* **144**, 133–147 (2019).
 21. Kuzmov, A. & Minko, T. Nanotechnology approaches for inhalation treatment of lung diseases. *J. Control Release* **219**, 500–518 (2015).
 22. Zhang, Y.-B. et al. A review of non-invasive drug delivery through respiratory routes. *Pharmaceutics* **14**, 1974 (2022).
 23. Yue, L. et al. Inhaled drug delivery: Past, present, and future. *Nano Today* **52**, 101942 (2023).
 24. Borghardt, J. M., Kloft, C. & Sharma, A. Inhaled therapy in respiratory disease: the complex interplay of pulmonary kinetic processes. *Can. Respir. J.* **2018**, 2732017 (2018).
 25. Rabiei, M. et al. Characteristics of SARS-CoV2 that may be useful for nanoparticle pulmonary drug delivery. *J. Drug Target.* **30**, 233–243 (2022).
 26. Arulmuthu, E. R., Williams, D. J., Baldascini, H., Versteeg, H. K. & Hoare, M. Studies on aerosol delivery of plasmid DNA using a mesh Nebulizer. *Biotechnol. Bioeng.* **98**, 939–955 (2007).
 27. Schneider, C. S. et al. Nanoparticles that do not adhere to mucus provide uniform and long-lasting drug delivery to airways following inhalation. *Sci. Adv.* **3**, e1601556 (2017).
 28. Esposito, C. et al. Advances in the cystic fibrosis drug development pipeline. *Life* **13**, 1835 (2023).
 29. Bai, X. et al. Inhaled siRNA nanoparticles targeting IL11 inhibit lung fibrosis and improve pulmonary function post-bleomycin challenge. *Sci. Adv.* **8**, eabn7162 (2022).
 30. Munoz-Lopez, P. et al. Single-chain fragment variable: recent progress in cancer diagnosis and therapy. *Cancers* **14**, 4206 (2022).
 31. Li, T. et al. A neutralization scFv antibody against IL-1 β isolated from a NIPA-based bacterial display library. *Curr. Pharm. Biotechnol.* **14**, 571–581 (2013).
 32. Ahmad, Z. A. et al. scFv antibody: principles and clinical application. *Clin. Dev. Immunol.* **2012**, 980250 (2012).
 33. Li, Z. et al. Enzyme-catalyzed one-step synthesis of ionizable cationic lipids for lipid nanoparticle-based mRNA COVID-19 vaccines. *ACS Nano* **16**, 18936–18950 (2022).
 34. Steckel, H., Eskandar, F. & Witthohn, K. The effect of formulation variables on the stability of nebulized aviscumine. *Int. J. Pharm.* **257**, 181–194 (2003).
 35. Hertel, S. P., Winter, G. & Friess, W. Protein stability in pulmonary drug delivery via nebulization. *Adv. Drug Deliv. Rev.* **93**, 79–94 (2015).
 36. Ghazanfari, T., Elhissi, A. M. A., Ding, Z. & Taylor, K. M. G. The influence of fluid physicochemical properties on vibrating-mesh nebulization. *Int. J. Pharm.* **339**, 103–111 (2007).
 37. McCallion, O. N. M., Taylor, K. M. G., Thomas, M. & Taylor, A. J. The influence of surface tension on aerosols produced by medical nebulisers. *Int. J. Pharm.* **129**, 123–136 (1996).
 38. Liu, N.-H. et al. Electrospinning of poly (ϵ -caprolactone-co-lactide)/ pluronic blended scaffolds for skin tissue engineering. *J. Mater. Sci.* **49**, 7253–7262 (2014).
 39. Gervasi, V. et al. Parenteral protein formulations: an overview of approved products within the European Union. *Eur. J. Pharm. Biopharm.* **131**, 8–24 (2018).
 40. Geng, Y. et al. PEAR1 regulates expansion of activated fibroblasts and deposition of extracellular matrix in pulmonary fibrosis. *Nat. Commun.* **13**, 7114 (2022).
 41. Viegi, G., Maio, S., Fasola, S. & Baldacci, S. Global burden of chronic respiratory diseases. *J. Aerosol Med. Pulm. Drug Deliv.* **33**, 171–177 (2020).
 42. Boardman, C. et al. Mechanisms of glucocorticoid action and insensitivity in airways disease. *Pulm. Pharmacol. Ther.* **29**, 129–143 (2014).
 43. Miravittles, M. & Anzueto, A. Chronic respiratory infection in patients with chronic obstructive pulmonary disease: what is the role of antibiotics? *Int. J. Mol. Sci.* **18**, 1344 (2017).
 44. Matera, M. G., Page, C. P., Calzetta, L., Rogliani, P. & Cazzola, M. Pharmacology and therapeutics of bronchodilators revisited. *Pharmacol. Rev.* **72**, 218–252 (2020).
 45. Secher, T. et al. Therapeutic antibodies: a new era in the treatment of respiratory diseases? *Pharmacol. Ther.* **189**, 149–172 (2018).
 46. Dentice, R. & Elkins, M. Timing of dornase alfa inhalation for cystic fibrosis. *Cochrane Database of Syst. Rev.* **3**, CD007923 (2011).
 47. De Groot, A. S. & Scott, D. W. Immunogenicity of protein therapeutics. *Trends Immunol.* **28**, 482–490 (2007).
 48. Rohner, E., Yang, R., Foo, K. S., Goedel, A. & Chien, K. R. Unlocking the promise of mRNA therapeutics. *Nat. Biotechnol.* **40**, 1586–1600 (2022).
 49. Suberi, A. et al. Polymer nanoparticles deliver mRNA to the lung for mucosal vaccination. *Sci. Transl. Med.* **15**, eabq0603 (2023).
 50. Zhang, H., Leal, J., Soto, M. R., Smyth, H. D. C. & Ghosh, D. Aerosolizable lipid nanoparticles for pulmonary delivery of mRNA through design of experiments. *Pharmaceutics* **12**, 1042 (2020).
 51. Lokugamage, M. P. et al. Optimization of lipid nanoparticles for the delivery of nebulized therapeutic mRNA to the lungs. *Nat. Biomed. Eng.* **5**, 1059–1068 (2021).
 52. Kim, J. et al. Engineering lipid nanoparticles for enhanced intracellular delivery of mRNA through inhalation. *ACS Nano* **16**, 14792–14806 (2022).
 53. Jiang, A. Y. et al. Combinatorial development of nebulized mRNA delivery formulations for the lungs. *Nat. Nanotechnol.* **19**, 364–375 (2024).
 54. Rowe, S. M. et al. Inhaled mRNA therapy for treatment of cystic fibrosis: Interim results of a randomized, double-blind, placebo-controlled phase 1/2 clinical study. *J. Cyst. Fibros.* **22**, 656–664 (2023).

55. Lee, Y., Jeong, M., Park, J., Jung, H. & Lee, H. Immunogenicity of lipid nanoparticles and its impact on the efficacy of mRNA vaccines and therapeutics. *Exp. Mol. Med.* **55**, 2085–2096 (2023).
56. Mu, X. & Hur, S. Immunogenicity of in vitro-transcribed RNA. *Acc. Chem. Res.* **54**, 4012–4023 (2021).
57. Elsadek, N. E., Abu Lila, A. S. & Ishida, T. Immunological responses to PEGylated proteins: anti-PEG antibodies. *Polymer-Protein Conjugates* **5**, 103–123 (2020).
58. Mohamed, M. et al. PEGylated liposomes: immunological responses. *Sci. Technol. Adv. Mater.* **20**, 710–724 (2019).
59. Gao, M. et al. Modulating Plaque inflammation via targeted mRNA nanoparticles for the treatment of atherosclerosis. *ACS Nano* **17**, 17721–17739 (2023).

Acknowledgements

The work was funded by “Open Competition to Select the Best Candidates” Key Technology Program for Nucleic Acid Drugs of NCTIB (NCTIB2022HS02002) and the National Key Research and Development Program of China (2023YFC2606003). X.X. acknowledges support from the National Science Foundation (2001606) and the Gustavus and Louise Pfeiffer Research Foundation Award.

Author contributions

X.-Q.Z., and X.X. conceived the project, supervised the research, and revised the manuscript. X.B. performed most experiments and wrote the original manuscript. Q.C. assisted with the design and preparations of iLNP. Y.T. synthesized the AA3-DLIn ionizable lipid. J.H. helped with the in vivo experiments. X.B., F.L., M.T., X.X. and X.-Q.Z. analyzed and discussed the results.

Competing interests

The authors declare no competing interests.

Additional information

Supplementary information The online version contains supplementary material available at <https://doi.org/10.1038/s41467-024-51056-8>.

Correspondence and requests for materials should be addressed to Xiaoyang Xu or Xue-Qing Zhang.

Peer review information *Nature Communications* thanks Achim Biesel, Aljoscha Gabelmann, Claus-Michael Lehr and the other, anonymous, reviewers for their contribution to the peer review of this work. A peer review file is available.

Reprints and permissions information is available at <http://www.nature.com/reprints>

Publisher’s note Springer Nature remains neutral with regard to jurisdictional claims in published maps and institutional affiliations.

Open Access This article is licensed under a Creative Commons Attribution-NonCommercial-NoDerivatives 4.0 International License, which permits any non-commercial use, sharing, distribution and reproduction in any medium or format, as long as you give appropriate credit to the original author(s) and the source, provide a link to the Creative Commons licence, and indicate if you modified the licensed material. You do not have permission under this licence to share adapted material derived from this article or parts of it. The images or other third party material in this article are included in the article’s Creative Commons licence, unless indicated otherwise in a credit line to the material. If material is not included in the article’s Creative Commons licence and your intended use is not permitted by statutory regulation or exceeds the permitted use, you will need to obtain permission directly from the copyright holder. To view a copy of this licence, visit <http://creativecommons.org/licenses/by-nc-nd/4.0/>.

© The Author(s) 2024